

A COMPREHENSIVE ANALYSIS OF THE *SWIFT*/XRT DATA:
II. DIVERSE PHYSICAL ORIGINS OF THE SHALLOW DECAY SEGMENT

EN-WEI LIANG^{1,2}, BIN-BIN ZHANG^{1,3}, BING ZHANG¹

Submitted to ApJ on April 29, 2007

ABSTRACT

The origin of the shallow decay segment in the *Swift*/XRT light curves is still a puzzle. We analyze the properties of this segment with a sample of 53 long *Swift* GRBs detected before Feb., 2007. We show that the distributions of its characteristics are log-normal or normal, and its isotropic X-ray energy ($E_{\text{iso,X}}$) is linearly correlated with the prompt gamma-ray energy, but with a steeper photon spectrum except for some X-ray flashes. No significant spectral evolution is observed from this phase to the follow-up phase, and the follow-up phase is usually consistent with the external shock models, implying that this shallow decay phase is also of external shock origin, likely due to a refreshed external shock. Within the refreshed shock model, the data are generally consistent with a roughly constant injection luminosity up to the end of this phase t_b . A positive correlation between $E_{\text{iso,X}}$ and t_b also favors the energy injection scenario. Among the 13 bursts that have well-sampled optical light curves, 6 have an optical break around t_b and the breaks are consistent with being achromatic. However, the other 7 bursts either do not show an optical break or have a break at a different epoch than t_b . This raises a concern to the energy injection scenario, suggesting that the optical and X-ray emissions may not be the same component at least for a fraction of bursts. There are 4 significant outliers in the sample, GRBs 060413, 060522, 060607A, and 070110. The shallow decay phase in these bursts is immediately followed by a very steep decay after t_b , which is inconsistent with any external shock model. The optical data of these bursts evolve independently from the X-ray data. These X-ray plateaus likely have an internal origin and demand continuous operation of a long-term GRB central engine. We conclude that the observed shallow decay phase likely has diverse physical origins.

Subject headings: radiation mechanisms: non-thermal: gamma-rays: bursts: X-rays

1. INTRODUCTION

The observations for the gamma-ray burst (GRB) phenomenon with the *Swift* satellite (Gehrels et al. 2004) have revolutionized our understanding on this phenomenon in many aspects (see recent reviews by Mészáros 2006; Zhang 2007). In its first two years of operation, the on-board X-ray telescope (XRT; Burrows et al. 2004) has accumulated a large set of well-sampled X-ray light curves from tens of seconds to days (even months) since the GRB triggers.

The generally accepted GRB models are the relativistic fireball models (Rees & Mészáros 1994; Mészáros & Rees 1997a; Sari et al. 1998; see reviews by Mészáros 2002; Zhang & Mészáros 2004; Piran 2005). This model invokes a fireball powered by a GRB central engine that ejects an intermittent, relativistic outflow. Internal shocks from stochastic collisions within the ejecta power the observed prompt gamma-rays, and deceleration of the fireball by the ambient medium excites a long term external forward shock that powers the broad band afterglow (Mészáros & Rees 1997a; Sari et al. 1998). Swift data suggest possible late internal shocks that are the origin of the erratic late X-ray flares seen in XRT light curves (Burrows et al. 2005; Zhang et al. 2006; Dai et al. 2006; Fan & Wei 2005; King et al. 2005; Proga & Zhang

2006; Perna et al. 2006). The XRT light curves generally begin with a rapidly decaying segment (Tagliaferri et al. 2005; O’Brien et al. 2006b), which is explained as the prompt emission tail due to the so-called “curvature effect” (Kumar & Panaitescu 2000b; Zhang et al. 2006; Liang et al. 2006; Yamazaki et al. 2006)⁴. The broadband afterglows, which usually decay as a power-law with an index of $\alpha \sim -1$ (normal decay phase), are believed to be related to the external shock. If the external shocks are refreshed by continuous energy injection into the blastwave, a shallow decay phase prior of the normal decay phase could be observed (Rees & Mészáros 1998; Dai & Lu 1998a,b; Panaitescu et al. 1998; Sari & Mészáros 2000; Zhang & Mészáros et al. 2001; Wang & Dai 2001; Dai 2004; Granot & Kumar 2006; Panaitescu 2007; Yu & Dai 2007; see Zhang 2007 for a review).

As the fireball is decelerated by the ambient medium, the normal decay phase transits to a jet-like decay phase (with a decay index $\alpha \sim -2$), when the bulk Lorentz factor is degraded to $\Gamma \sim \theta_j^{-1}$, where θ_j is the opening angle of a conical jet (Rhoads 1997; Sari et al. 1999). Therefore, four successive emission episodes are invoked in the framework of the fireball models, i.e., prompt gamma-ray phase with a tail, shallow decay phase, normal decay phase, and jet-like decay phase. These power law segments, together with erratic X-ray flares, composes a canonical X-ray afterglow lightcurve revealed by Swift (Zhang et al. 2006; Nousek et al. 2006; O’Brien et al.

¹ Department of Physics and Astronomy, University of Nevada, Las Vegas, NV 89154, USA; lew@physics.unlv.edu; zbb@physics.unlv.edu; bzhang@physics.unlv.edu

² Department of Physics, Guangxi University, Nanning 530004, China

³ National Astronomical Observatories/Yunnan Observatory, CAS, Kunming 650011, China

⁴ Other suggestions to interpret this segment include cooling of a hot cocoon surrounding the GRB jet (Pe’er et al. 2006) or a highly radiative blast wave (Dermer 2007).

2006b). The physical origins of these segments have been discussed in the literature (Zhang et al. 2006; Nousek et al. 2006; Panaitescu et al. 2006a). Empirically, O’Brien et al. (2006a,b) and Willingale et al. (2007) show that the data can be fitted by the superposition of a prompt emission component and an afterglow component.

In order to explore the physical origin of this canonical afterglow lightcurve, we perform a systematic analysis of the Swift XRT data. In the first paper of this series (Zhang, Liang, & Zhang 2007, Paper I of this series), we have studied the steep decay phase for a sample of bright tails, and revealed an apparent hard-to-soft spectral evolution for some bursts (see also Campana et al. 2006; Mangano et al. 2007; Butler & Kocevski 2007). This paper will focus on the shallow decay phase and the subsequent phase. This is motivated by some puzzling facts related to the shallow decay phase. For example, simultaneous X-ray/optical observations suggest that the break between the shallow and the normal decay segments in the X-ray band for some GRBs is chromatic (Panaitescu et al. 2006b; Fan & Piran 2006). This is inconsistent with the simplest energy injection model. One fundamental question is whether X-ray and optical afterglows have the same physical origin. Another interesting fact is that the XRT light curve of GRB 070110 shows a long-lived plateau followed by an abrupt fall-off (the decay slope ~ -9 with zero time at the trigger time). This feature is hard to interpret within the external shock models, and it likely indicates a long-lasting central engine emission component (Troja et al. 2007).

Theoretically, several models have been proposed to interpret the shallow decay phase (e.g. Zhang 2007 for a review). Besides the energy injection models (Zhang et al. 2006; Nousek et al. 2006; Panaitescu et al. 2006a), other models include the combination of the GRB tail with the delayed onset of the afterglow emission (Kobayashi & Zhang 2007); off-beam jet model (Toma et al. 2006; Eichler & Granot 2006); pre-cursor model (Ioka et al. 2006); two-component jet (Granot et al. 2006; Jin et al. 2007), varying microphysics parameter model (Ioka et al. 2006; Panaitescu et al. 2006b; Fan & Piran 2006; Granot et al. 2006), etc. The chromaticity of some X-ray shallow-to-normal breaks drives several ideas that go beyond the traditional external forward shock model. For example, Shao & Dai (2007) interpret the X-ray lightcurve as due to dust scattering of some prompt X-rays, so that it has nothing to do with the external shock. Uhm & Beloborodov (2007) and Genet, Daigne & Mochkovitch (2007) interpret both X-ray and optical afterglow as emission from a long-lived reverse shock. Ghisellini et al. (2007) even suggested that the shallow-to-normal transition X-ray afterglows may be produced by late internal shocks, and the end of this phase is due to the jet effect in the prompt ejecta (see also Nava et al. 2007).

The observational puzzles and theoretical chaos call for a systematic understanding of the shallow decay phase data for a large sample of GRBs. In particular, it is desirable to find out how bad the standard external forward shock model is when confronted with the data, e.g. what fraction of bursts actually call for models beyond the standard external forward shock model. This is the primary goal of this paper. Data reduction and sample selection are presented in §2. The characteristics of

the shallow decay segment and their relations with the prompt gamma-ray phase are explored in §3. In §4, we test the external origin of the power law segment following the shallow decay phase and explore whether or not the shallow decay segment is also of external origin. Assuming an energy injection model for shallow decay phase, we further analyze the the energy injection model parameters of these bursts in §5. The relation among the isotropic X-ray energy ($E_{\text{iso,X}}$), peak energy of the prompt gamma-ray νf_ν spectrum (E_p), and t_b is investigated in §6. The results are summarized in §7 with some discussion. Throughout the paper the cosmological parameters $H_0 = 71 \text{ km s}^{-1} \text{ Mpc}^{-1}$, $\Omega_M = 0.3$, and $\Omega_\Lambda = 0.7$ have been adopted.

2. DATA REDUCTION AND SAMPLE SELECTION

The XRT data are taken from the Swift data archive. We developed a script to automatically download and maintain all the XRT data. The *Heasoft* packages, including *Xspec*, *Xselect*, *Ximage*, and *Swift* data analysis tools, are used for the data reduction. We have developed an IDL code to automatically process the XRT data for a given burst in any user-specified time interval. Our procedure is described as follows. The details of our code have been presented in Paper I.

Our code first runs the XRT tool *xrtpipeline* to reproduce the XRT clean event data, and then makes pile-up corrections with the same methods as discussed in Romano et al. (2006) (for the Window Timing [WT] mode data) and Vaughan et al. (2006) (for the Photon Counting [PC] mode data). Both the source and background regions are annuli (for PC) or rectangular annuli (for WT). The inner radius of the (rectangular) annuli are dynamically determined by adjusting the inner radius of the annuli through fitting the source brightness profiles with the King’s point source function (for PC) or determined by the photon flux using the method described in Romano et al 2006 (for WT). If the pipe-up effect is not significant, the source regions are in the shape of a circle with radius $R = 20$ pixels (for PC) or of a 40×20 pixels rectangle (for WT) centered at the bursts’ positions. The background regions have the same size as the source region, but has a distance of 20 pixels away from the source regions. The exposure correction is also made with an exposure map created by XRT tools *xrtexpomap*. By considering these corrections, the code extracts the background-subtracted light curve and spectrum for the whole XRT data set. The signal-to-noise ratio is normally taken as 3σ , but it is not rigidly fixed at this value and may be flexibly adjusted depending on the source brightness.

With our code we process all the XRT data observed between Feb., 2005 and Jan., 2007. We inspect all the light curves to identify the beginning (t_1) of the shallow decay segment and the end (t_2) of the decay phase following the shallow phase (which usually is the normal decay phase, but in some cases the decay slope could be much steeper). Please note that the selection of t_1 and t_2 is guided by eye without a rigid criterion. Generally, t_1 is taken as the end of the steep decay segment or the beginning of the observation time, unless significant flares or high level emission bumps following the GRB tails were observed. The ending time t_2 is taken as the end of the observation time except for GRBs 050416A, 050803,

060413, 060908, 060522, 061121, and 070110, which have an additional break at later times, and t_2 is chosen as that break time. For example, GRBs 060522 and 070110 have a distinct “normal-decay” emission component following the sharp decay segment, and t_2 is taken the end of the sharp decay. The last data points of GRB 050416A, 050803, 060413, 060908, and 061121 show a flattening feature, which significantly deviates from the power law decay trend post t_b . We thus do not include those data points.

Physically, the temporal break of an external shock origin should be smooth (due to the equal-arrival-time effect of a relativistic shell of conical geometry). Therefore, a smoothed broken power law is used to fit the light curve in the time interval $[t_1, t_2]$,

$$F = F_0 \left[\left(\frac{t}{t_b} \right)^{\omega\alpha_1} + \left(\frac{t}{t_b} \right)^{\omega\alpha_2} \right]^{-1/\omega}, \quad (1)$$

where ω describes the sharpness of the break. The larger the ω , the sharper the break. In order to constrain ω it is required that the time interval covers a range from $t_1 \ll t_b$ to $t_2 \gg t_b$, and that the light curve around t_b is well-sampled. The parameter t_b is not significantly affected by ω , but both α_1 and α_2 are. We show the comparison of the fitting results with $\omega = 1$ and $\omega = 3$ for the bursts in our sample (see below) in Fig. 1. We find that systematically, $t_b^{\omega=1} \sim t_b^{\omega=3}$, $\alpha_1^{\omega=1} < \alpha_1^{\omega=3}$, and $\alpha_2^{\omega=1} > \alpha_2^{\omega=3}$. We notice that Willingale et al. (2007) fit the XRT light curves with a superposition model of both the prompt and afterglow emission components. The derived α_2 from our fitting with $\omega = 3$ is generally consistent with their results. We therefore fix $\omega = 3$ in this analysis, except for GRBs 060413, 060522, 060607A, and 070710. The XRT light curves of these bursts abruptly drop at t_b , and we take $\omega = 10$. We then create a time filter array that contains two time intervals of $[t_1, t_b]$ and $[t_b, t_2]$ for each burst. By specifying the time filter array we run our code again to extract the spectra in the two time intervals and derive their photon indices, $\Gamma_{X,1}$ and $\Gamma_{X,2}$, by fitting the spectra with a power law model incorporating with absorptions by both the Milky Way Galaxy and the host galaxy, $wabs^{\text{Gal}} \times zwabs^{\text{host}} \times$ power law (when the redshift is unknown, $zwabs^{\text{host}}$ is replaced with the model of $wabs$). The N_H^{host} value in the time-resolved spectral analysis is fixed to the value obtained from fitting the time-integrated spectrum during the whole time span of each burst.

The t_b is roughly considered as the duration of the shallow decay phase. As suggested by Lazzati & Begelman (2006) and Kobayashi & Zhang (2007), the zero time of the external-origin power-law segments should be roughly the BAT trigger time. In our calculation, in order to account for the onset of the afterglow we take a t_0 as 10 seconds after the GRB trigger. The X-ray fluence (S_X) of the shallow decay phase is derived by integrating the fitting light curve from 10 seconds post the GRB trigger to t_b without considering the contributions of both early X-ray flares and the GRB tail emissions. Since the shallow decay phase has a temporal decay index shallower than -1, the results are not sensitive to the choice of t_0 . We estimate the uncertainty of S_X with a bootstrap method based on the errors of the fitting parameters, assuming that the errors of the fitting parameters, $\sigma_{\log F_0}$, $\sigma_{\log t_b}$, σ_{α_1} , and σ_{α_2} , are of Gaussian

distributions. We generate 5×10^3 parameter sets of $(F_0, t_b, \alpha_1, \alpha_2)$ from the distributions of these parameters for each burst, and then calculate S_X for each parameter set. We make a Gaussian fit to the distribution of $\log S_X$ and derive the central value of $\log S_X$ and its error $\sigma_{\log S_X}$. In our fittings, α_1 and/or t_b are fixed for GRBs 050801 and 060607A. We do not calculate the errors for the two bursts.

We use the following criteria to select our sample. First, the XRT light curves have a shallow decay segment following the GRB tails. Since the decay slope of the “normal” decay phase predicted by the external GRB models is generally steeper than 0.75, we require that the so-called shallow decay segment has a slope $\alpha_{X,1} < 0.75$ at 1σ error. Second, both the shallow decay segment and the follow-up segment are bright enough to perform spectral analysis. Systematically going through all the *Swift* XRT data before Feb. 2007 we use the above criteria to compile a sample of 53 bursts. Please note that the apparently long GRB 060614 is also included in our sample, although it may belong to the short-type bursts (Gehrels et al. 2006; Zhang et al. 2007b; Zhang 2006). The XRT light curves and the fitting results are shown in Fig. 2, and the data are summarized in Table 1. We collect the BAT observations of these bursts from GCN circular reports, and report them in Table 2. We search the optical afterglow data of these bursts from published papers and GCN circular reports⁵. We identify a burst as optically bright, if three or more detections in the UV-optical bands were made. We find that 30 out of the 53 bursts are optically bright, but only 15 bursts have an optical light curve with good temporal coverage. We make the Galactic extinction correction and convert the observed magnitudes to energy fluxes. We fit these light curves with a simple power law or the smooth broken power law (ω is also fixed as 3). The fitting results are summarized in Table 3. We directly compare the optical data with the XRT data in Fig. 2 in order to perform a quick visual check of achromaticity of these light curves. If multi-wavelength optical light curves are available, we show only the one that was observed around the X-ray shallow decay phase with the best sampling. Notice that the contribution from the host galaxy to the optical light curve of GRB 060614 has been removed.

Twenty-seven out of the 53 GRBs in our sample have redshift measurements. Table 4 reports the properties of these bursts in the burst rest frame, including the durations (T'_{90} and t'_b) and the equivalent-isotropic radiation energies ($E_{\text{iso},\gamma}$ and $E_{\text{iso},X}$) in the prompt phase and in the shallow decay phase, and the peak energy of the νf_ν spectrum (E'_p). The $E_{\text{iso},\gamma}$ and $E_{\text{iso},X}$ are calculated by

$$E_{\text{iso},(\gamma,X)} = \frac{4\pi D_L^2 S_{(\gamma,X)}}{1+z}, \quad (2)$$

where S_γ is the gamma-ray fluence in the BAT band and S_X is the X-ray fluence in the shallow decay phase in the XRT band, and D_L is the luminosity distance of the source. Due to the narrowness of the BAT band, the BAT data cannot well constrain the spectral parameters of GRBs (Zhang et al. 2007a). Generally the BAT spectrum can be fitted by a simple power law, and the power

⁵ The GRBLog web page (<http://grad40.as.utexas.edu/grblog.php>) has been used.

law index Γ is correlated with E_p (Zhang et al. 2007b; see also Sakamoto et al. 2007; Cabrera et al. 2007)⁶, i.e.,

$$\log E_p = (2.76 \pm 0.07) - (3.61 \pm 0.26) \log \Gamma. \quad (3)$$

We estimate E_p with this relation if it is not constrained by the BAT data. We then calculate the *bolometric* energy $E_{\text{iso},\gamma}^b$ in the $1 - 10^4$ keV band with the k -correction method used by Bloom et al. (2001), assuming that the photon indices are -1 and -2.3 before and after E_p , respectively (Preece et al. 2000). Both E_p' and $E_{\text{iso},\gamma}^b$ are listed in Table 4.

3. THE CHARACTERISTICS OF THE SHALLOW DECAY PHASE AND ITS RELATIONS TO THE PROMPT GAMMA-RAY PHASE

We display the distributions of the characteristics of the shallow decay phase in Fig. 3. It is found that these distributions are consistent with being normal/lognormal, i.e. $\log t_b/s = 4.09 \pm 0.61$, $\log S_X/\text{erg cm}^{-2} = -6.52 \pm 0.69$, $\Gamma_{X,1} = 2.09 \pm 0.21$, and $\alpha_1 = 0.35 \pm 0.35$. Quoted errors are at 1σ confidence level.

We investigate the relation of the shallow decay phase to the prompt gamma-ray phase. Figure 3 shows t_b , S_X , $\Gamma_{X,1}$, and $E_{\text{iso},X}$ as functions of T_{90} , S_γ , Γ_γ , and $E_{\text{iso},\gamma}$, respectively. No correlation between Γ_γ and $\Gamma_{X,1}$ is observed. However, $\Gamma_{X,1}$ is larger than Γ_γ , except for some X-ray flashes (XRFs), indicating that the photon spectrum of the shallow decay phase is generally steeper than that of the prompt gamma-ray phase for typical GRBs. It is interesting to note that in contrast to Γ_γ $\Gamma_{X,1}$ is narrowly clustered around 2.1 (see also O'Brien et al. 2006a), hinting a possible common microscopic mechanism during the shallow decay phase.

From Fig. 3 we find tentative correlations of durations, energy fluences, and isotropic energies between the gamma-ray and X-ray phases. The best fits yield $\log t_b = (0.61 \pm 0.16) \log T_{90} + (3.00 \pm 0.27)$ ($r = 0.48$ and $p = 0.003$ for $N = 53$), $\log S_X = (0.76 \pm 0.11) \log S_\gamma + (-2.33 \pm 0.60)$ ($r = 0.70$ and $p < 10^{-4}$ for $N = 53$), and $\log E_{\text{iso},X} = (1.00 \pm 0.16) \log E_{\text{iso},\gamma} + (-0.50 \pm 8.10)$ ($r = 0.79$ and $p < 10^{-4}$ for $N = 27$). It is found that t_b weakly depends on T_{90} . However, X-ray fluence and isotropic energy are almost linearly correlated with gamma-ray fluence and gamma-ray energy, respectively. $E_{\text{iso},\gamma}$ is greater than $E_{X,\text{iso}}$ for most of the bursts, but for a few cases $E_{\text{iso},X}$ is even larger than $E_{\gamma,\text{iso}}$. In order to reveal possible linear correlations for the quantities in the two phases, we define a 2σ linear correlation regions with $y = x + (A \pm 2 \times \sigma_A)$, where y and x are the two quantities in question, and A and σ_A are the mean and its 1σ standard error of the $y - x$ correlation, respectively. The 1σ regions of the correlations are shown with dashed lines in Fig. 4. These results indicate that radiation during the shallow decay phase is correlated with that in the prompt gamma-ray phase.

4. TESTING THE PHYSICAL ORIGIN OF THE SHALLOW DECAY SEGMENT USING THE PROPERTIES OF THE FOLLOW-UP SEGMENT

⁶ We should point out that this empirical relation is for BAT observations only. The origin of this relation is due to the narrowness of the BAT instrument. It can be robustly used for those bursts whose E_p are roughly within the BAT band.

The leading scenario of the shallow decay phase is a refreshed forward shock due to either a long-term central engine or a spread of the ejecta Lorentz factor (Zhang et al. 2006; Nousek et al. 2006; Rees & Mészáros 1998; Dai & Lu 1998a,b; Zhang & Mészáros 2001; Granot & Kumar 2006; Yu & Dai 2007). Within such a scenario, the shallow decay phase ends at t_b and transits to a “normal” decay phase consistent with the standard external forward shock models. Three criteria are required to claim an energy injection break t_b . First, there should be no spectral evolution across t_b since energy injection is a pure hydrodynamical effect. Second, due to the same reason, the break at t_b should be achromatic. Third, the power-law decay phase after t_b should comply with the standard external shock models. In this section, we test whether all three criteria are satisfied with the data.

Figure 4(a) shows $\Gamma_{X,2}$ as a function of $\Gamma_{X,1}$. The solid line is $\Gamma_{X,2} = \Gamma_{X,1}$, and the dashed lines marks the 3σ region of the equality, which is defined with $\Gamma_{X,2} = \Gamma_{X,1} + (\mathcal{G} \pm 3\delta_{\mathcal{G}})$, where \mathcal{G} and $\delta_{\mathcal{G}}$ are the mean and statistical uncertainty (1σ level) of the difference $\Gamma_{X,2} - \Gamma_{X,1}$. Please note that $\delta_{\mathcal{G}}$ does not include the observational uncertainty. It statistically describes the scatter of \mathcal{G} for the bursts in our sample. We find that only one burst GRB 061202 is out of the region. The comparison between the distributions of $\Gamma_{X,2}$ and $\Gamma_{X,1}$ is shown in Fig. 4(b). Excluding GRB 061202, the two distributions are consistent. The Kolmogorov-Smirnov test suggests that the significance level of this consistency is 0.96. These results indicate that $\Gamma_{X,1}$ and $\Gamma_{X,2}$ for the bursts in our sample are globally consistent with each other. In order to verify this consistency within observed uncertainty for individual bursts, Fig. 4(c) shows the distribution of the ratio $\mu = \mathcal{G}/\sigma$, where $\sigma^2 = \delta\Gamma_{X,1}^2 + \delta\Gamma_{X,2}^2$ is the observed uncertainty of \mathcal{G} . A positive value of μ would indicate a hard-to-soft spectral evolution. This ratio indicates the significance level of the difference between $\Gamma_{X,1}$ and $\Gamma_{X,2}$ for individual bursts within the observational uncertainties of the two quantities. As shown in Fig. 4(c), most of the bursts ($\sim 90\%$) have $\mu \lesssim 1$, and only one burst (GRB 061202) has $\mu > 3$. These results prove that no significant spectral evolution between the two phases with a confidence level above 3σ is observed for the bursts in our sample within the observational error, except for GRB 061202. This is consistent with the expectation of the refreshed shock afterglow models. Please note that GRB 061202 shows significant hard-to-soft spectral evolution from the shallow to the normal decay phases, i.e., from $\Gamma_{X,1} = 2.25 \pm 0.07$ to $\Gamma_{X,2} = 3.55 \pm 0.44$. One caveat for this spectral evolution is that there is a long observational gap between the first epoch in the shallow decay phase (4×10^3 to 2×10^4 seconds) and the second epoch in normal decay phase ($1 \times 10^5 \sim 5 \times 10^5$ seconds) when the spectral indices are measured. Without detecting the break itself, it may be dangerous to draw the conclusion that spectral variation is clearly seen across t_b . We cannot rule out the possibility that the plateau extends further and drops dramatically before landing onto a normal decay segment as is seen in GRBs 060522 and 070110 (see discussion below).

Although the mechanism of energy injection into the forward shock could vary (e.g. Rees & Mészáros 1998; Dai

& Lu 1998a,b; Zhang & Mészáros et al. 2001; Yu & Dai 2007), the kinetic energy of the fireball after the energy injection is over should be constant and this “normal” decay phase should be explained with the standard external shock models. Without broadband afterglow modeling, the “closure relations” between the observed spectral index β and temporal decay index α present a simple test to the models. In Fig.5, we present $\alpha_{X,2}$ as a function of spectral index $\beta_{X,2}$, where $\beta_{X,2} = \Gamma_{X,2} - 1$. The closure correlations of the external shock afterglow models for different spectral regimes, different cooling schemes, different ambient medium properties, and different electron distributions (the spectral index $p > 2$ and $p < 2$) are shown in Fig. 5 (see Table 1 of Zhang & Mészáros 2004 and reference therein, in particular Sari et al. 1998; Chevalier & Li 2000; Dai & Cheng 2001). The fact that the observed $\beta_{X,2}$ is greater than 0.5 for the bursts in our sample suggests that these X-rays are in the spectral regime $\nu_X > \max(\nu_m, \nu_c)$ (Regime I) or $\nu_m < \nu_X < \nu_c$ (Regime II), where ν_m and ν_c are the characteristic frequency and cooling frequency of synchrotron radiation. The relation between α and β for the spectral Regime I is $\alpha = (3\beta - 1)/2$ regardless of the type of the medium (ISM or wind medium). If the X-ray band is in the Regime II, we have $\alpha = 3\beta/2$ (for ISM) and $\alpha = (3\beta + 1)/2$ (for wind). We define

$$D = |\alpha^{\text{obs}} - \alpha(\beta^{\text{obs}})|, \\ \delta_D = \sqrt{(\delta\alpha^{\text{obs}})^2 + [\delta\alpha(\beta^{\text{obs}})]^2}, \quad (4)$$

where $\alpha^{\text{obs}}(\delta\alpha^{\text{obs}})$ and $\alpha(\beta^{\text{obs}})$ are the temporal decay slopes (errors) from the observations and from the closure relations. The ratio $\phi = D/\delta_D$ reflects the “nearness” of the data point to the model predictions within the error scope. If $\phi < 1$, we consider that the data point goes cross the corresponding closure relation line. If $\phi < 3$, we regard that the model cannot be excluded within a 3σ significance level. Those bursts that have large uncertainties on both α and β may be interpreted with more than one models. In this case, we compare ϕ values derived from these models and take the model that gives the smallest ϕ .

As shown in Fig. 5, 24 out of the 53 bursts distribute around the line for the spectral Regime I. A group of bursts have a decay slope shallower than the model prediction, but they are slightly below and almost keep abreast with the Regime I model line (see also Fig. 5 of Willingale et al. 2007). At the 3σ confidence level, this model cannot be excluded for these bursts. Eighteen bursts are consistent with the ISM external shock afterglow model in the spectral regime II.

Six bursts (GRBs 050315, 050318, 050803, 060614, 051008, and 060906) agree with both the regime I ISM jet model and the regime II wind model. The observed β of these six bursts are ~ 1 . The two models are almost degenerate at $\beta \sim 1$. We therefore use the spectral and temporal behaviors of the prior segment to distinguish the two models. Since the observed $\beta > 0.5$ in our sample, the decay slope of the light curves before a jet break should be steeper than $(3\beta)/2 \sim 0.75$. From Table 1 we can see that the α_1 values are 0.66 ± 0.03 , 0.90 ± 0.23 , 0.25 ± 0.03 , 0.18 ± 0.06 , 0.78 ± 0.11 , and 0.35 ± 0.10 , respectively, for the six bursts. So there is no confident evidence to claim a jet break within the un-

certainty of the decay slope for these bursts⁷ Since the energy injection model the shallow decay slope depends on a free parameter q , we tentatively suggest that these six cases can be explained with a wind afterglow model in the spectral regime II. GRB 060108 is also consistent with this model according to our criterion.

As shown above, the spectral index and temporal decay slope of the normal decay phase for most bursts in our sample (49 out of 53 bursts) are roughly consistent with the closure relations of the external shock models. This further favors the idea that the shallow decay segment is also of external shock origin, and probably is related to a long-term energy injection effect. In this scenario, the energy injection break should be achromatic, if the multi-wavelength radiations are all from the same emission region, presumably the forward shock. We therefore inspect the optical light curves of these bursts to examine whether the breaks observed in the XRT light curves are achromatic. Among these 13 bursts have well-sampled optical light curves, as shown in Fig. 2 and Table 3. The optical light curves of GRBs 050801, 051109A, 060614, 060714, 060729, and 061121 show a break around t_b , indicating that the breaks in both the X-ray and the optical bands are consistent with being achromatic. However, the optical light curves of GRBs 050318, 050319, 050802, 060124, and 050401 do not have a break around t_b (see also Panaitescu et al. 2006b). They can be well fitted by a simple power law model. GRBs 060210 and 060526 have an optical break, but the breaks are not around t_b .

GRBs 060413, 060522, 060607A, and 070110 have a plateau with a step-like sharp drop ($\omega = 10$ is required in our data fitting). Except for GRB 060522, the other three bursts deviate significantly from any external shock afterglow models at 3σ significance level. Although the sharp drop segment of GRB 060522 is consistent with the regime II, wind-jet model, the plateau convincingly rules out this model since it cannot be explained as the pre-jet segment within the same model. These results suggest that the sharp drop segment and its prior plateau in these bursts are very likely not of external shock origin. A direct support to this speculation is that the optical lightcurves of these bursts, if available, are all evolve independently with respect to the X-ray lightcurves. For example, The optical light curve of GRB 060607A rapidly increases (with $F \propto t^3$) up to a maximum at $t = 160$ seconds post the GRB trigger, and then continuously decays with an index of -1.18 ± 0.02 (Molinari et al. 2007). The X-ray lightcurve, on the other hand, shows significant flares before 600 seconds, and a plateau lasting from 600 seconds to $\sim 1.2 \times 10^4$ seconds after the GRB trigger. At the end of the plateau, the XRT light curve drops

⁷ The possibility that a jet break is temporarily coincident with an energy injection break is however not ruled out. The normal decay phase could be missed in data fitting, if the normal decay segment is short, the data is sparse, or the jet break is not significant (e.g. Wei & Lu 2000; Kumar & Panaitescu 2000a; Gou et al. 2001). One example of this scenario is GRB 060614. Our best fit with a smooth broken power law does not reveal a jet-like break from a normal decay phase. However, Mangano et al. (2007) suggest a normal decay phase between 3.66×10^4 and 1.04×10^5 seconds by fitting the light curve with a joint-power-law model (the breaks are guided by eye). They showed that the decay slope during the period is 1.03 ± 0.02 . This normal decay phase thus satisfies a closure relation of the standard forward shock models. For a detailed study of jet breaks please see our paper III in the series, E.-W. Liang et al. 2007, in preparation.

sharply with $\alpha_2 = 3.35 \pm 0.09$. During the plateau in the XRT light curve, the optical light curve “normally” decays until a significant flare around 2000 seconds. The optical light curve is consistent with an external forward shock, and the peak is consistent with onset of the afterglow (Molinari et al. 2007). The plateau and the sharp drop in the XRT light curve of GRB 070110 is similar to that of GRB 060607A, but an additional “normal”-decay component post the steep fall-off was also observed (Troja et al. 2007). The decay slope of this late X-ray emission component is similar to that of the optical light curve and is likely of external shock origin (see also GRB 060522). This reinforces the suggestion that the early X-ray plateau is of internal origin and is connected to a long-lasting central engine (Troja et al. 2007). A common signature of these internal-origin plateaus is that the flux almost keeps constant on the plateau but with significant flickering. Although it may not be unreasonable to interpret it as late internal shocks (which usually give rise to erratic collisions within the ejecta and may power X-ray flares), another possibility is that the plateau is powered by tapping the spindown energy of the central engine, as suggested by Troja et al. (2007).

5. ENERGY INJECTION BEHAVIOR

As shown above, the normal decay phase for most of the bursts in our sample (49 out of 53) are consistent with the external shock models. This suggests that, in general, the observed shallow decay phase is also of the external origin and may be related to continuous energy injection into the fireball. In this section, we assume the standard energy injection model and infer from the data the parameters of the long-lived central engine.

We describe the energy injection behavior as $L(t) \propto t^{-q}$ (e.g. Zhang & Mészáros 2001)⁸. The difference between the decay slopes before and after t_b depends on the observed spectral regime and the type of ambient medium, which can be summarized as (derived from Table 2 of Zhang et al. 2006),

$$\Delta\alpha = \begin{cases} \frac{(p+2)(1-q)}{4}, & \text{spectral regime I, ISM and Wind,} \\ \frac{(p+3)(1-q)}{4}, & \text{spectral regime II, ISM,} \\ \frac{(p+1)(1-q)}{4}, & \text{spectral regime II, Wind,} \end{cases} \quad (5)$$

where p is the power law index of the electron distribution. The p value is derived from the observed spectral index, depending on the observed spectral regime. We identify the spectral regime for these bursts by comparing the observed $\alpha_{X,2}$ and $\beta_{X,2}$ with the closure correlations, and then derive their q values from Eqs. 5. The distributions of these GRBs in the two dimensional $q - \Delta\alpha$ and $q - p$ planes are shown in Fig. 6, along with the contours of constant p and $\Delta\alpha$ lines derived from the models (Eq.[5]). No correlation between α_1 and α_2 is found. The steepening index $\Delta\alpha$ is found to vary among bursts, with an average of 1.11 ± 0.39 . The p values range from $2 \sim 3.5$ without evidence of clustering (see

⁸ Another injection scenario invoking a distribution of the Lorentz factor of the ejecta (Rees & Mészáros 1998) can be effectively represented by a long-term central engine (Zhang et al. 2006). The internal-origin plateaus discussed above suggest that at least for some GRBs, a long-lived central engine is indeed in operation.

also Shen et al. 2006). The q values for most bursts are around -0.75 to 0.55 , with an average of $\sim -0.07 \pm 0.35$. It is worth commenting that a specific energy injection model invoking a spindown pulsar predicts a q value of 0 (Dai & Lu 1998a; Zhang & Mészáros 2001). The average q value is close to this model prediction.

6. EMPIRICAL RELATION AMONG $E_{\text{ISO}} - E_p - T_B$

An empirical relation among $E_{\text{iso}} - E'_p - t'_{b,opt}$ was discovered with pre-Swift GRBs, where $t'_{b,opt}$ is the temporal break of the optical afterglow light curve in the rest frame of the burst (Liang-Zhang relation; Liang & Zhang 2005)⁹. Willingale et al. (2007) found a similar correlation to the Ghirlanda relation by assuming that t_b in the X-ray band are jet breaks. Such a relation may be interpreted as an effective $E_{\text{iso}} - E'_p - t'_b$ relation similar to the Liang-Zhang relation. In this section we investigate the relations among the energies $E_{\text{iso},\gamma}^b$, $E_{\text{iso},X}$ and the other two parameters E'_p and t'_b . With the data reported in Table 4 (for bursts with redshift measurements), we use a multi-variable regression analysis method to search for possible dependences of $E_{\text{iso},X}$ and $E_{\text{iso},\gamma}^b$ on both E'_p and t'_b . Our sample is limited to those bursts whose t_b can be explained as an energy injection break (without considering the achromaticity of the break). Among the 49 bursts 27 have redshift measurements. Since only two bursts in the internal-origin plateau sample have redshift measurements, we cannot make an analysis to them. Our regression model reads

$$\log \hat{E}_{\text{iso}} = \kappa_0 + \kappa_1 \log E'_p + \kappa_2 \log t'_b \quad (6)$$

where $E'_p = E_p(1+z)$ and $t'_b = t_b/(1+z)$. We measure the significance level of the dependences of each variable on the model by the probability of a t-test (p_t). The significance of the global regression is measured by a F-test (with a chance probability p_F). Statistically, a robust statistical analysis requires the chance probability to be less than 10^{-4} . Our multiple regression analysis to $E_{\text{iso},X}(E'_p, t'_b)$ shows $\kappa_0 = 44.0 \pm 1.1$ (with $p_t < 10^{-4}$), $\kappa_1 = 1.82 \pm 0.33$ (with $p_t < 10^{-4}$), and $\kappa_2 = 0.61 \pm 0.18$ (with $p_t = 3 \times 10^{-3}$). The p_F is $< 10^{-4}$. These results suggest a strong correlation between $E_{\text{iso},X}$ and E'_p and a tentative correlation between $E_{\text{iso},X}$ and t'_b . On the other hand, our multiple regression analysis to $E_{\text{iso},\gamma}^b(E'_p, t'_b)$ gives $\kappa_0 = 48.3 \pm 0.8$ (with $p_t < 10^{-4}$), $\kappa_1 = 1.70 \pm 0.25$ (with $p_t < 10^{-4}$), and $\kappa_2 = 0.07 \pm 0.13$ (with $p_t = 0.486$). The p_F is $< 10^{-4}$. It is found that the correlation between $E_{\text{iso},\gamma}^b$ and E'_p is significant, but statistically no correlation between $E_{\text{iso},\gamma}^b$ and t'_b can be claimed.

With the relation discovered by Willingale et al. (2007), one would naively expect a multi-variable correlation among $E_{\text{iso},\gamma}^b - E'_p - t'_b$. According to our results, a significant correlation among $E_{\text{iso},\gamma}^b - E'_p - t'_b$ could be indeed claimed with a chance probability $p_F < 10^{-4}$.

⁹ If $t'_{b,opt}$ is interpreted as a jet break, then the relation is similar to the Ghirlanda-relation (Ghirlanda et al. 2004). However, the more empirical Liang-Zhang relation allows more freedom to understand the origin of the breaks.

However, this correlation is dominated by the correlation of $E_{\text{iso},\gamma}^b - E_p'$ only (with a $p_t < 10^{-4}$), which is essentially the Amati-relation (Amati et al. 2002). The p_t of the dependence between $E_{\text{iso},\gamma}^b$ and t_b' is 0.486. This strongly rules out such a dependence. Therefore, we suspect that the apparent relation found by Willingale et al. (2007) would be intrinsically a manifestation of the Amati-relation. A similar conclusion has been also achieved by Nava et al. (2007). The t_b essentially did not enter the problem, since the distribution of t_b is narrower than that of $t_{b,\text{opt}}$ as discussed in Liang & Zhang (2005).

It is interesting to note the dependence $E_{\text{iso},X} \propto t_b'^{0.61 \pm 0.18}$. This is in sharp contrast to the Liang-Zhang relation, in which $E_{\text{iso},\gamma} \propto t_{b,\text{opt}}'^{-1.24}$ was discovered. In order to compare the $E_{\text{iso},X} - E_p' - t_b'$ correlation with the Liang-Zhang relation in a 2-dimensional plane, we define $\Sigma = \log E_{\text{iso},X} - \kappa_2 \log t_b'$, and show Σ_X and Σ_γ as a function of $\log E_p'$ in Fig. 8. We observe that the $E_{\text{iso},X} - E_p' - t_b'$ correlation is significant, but it has a larger scatter than the Liang-Zhang relation. Although we can not rule out the possibility that the large dispersion is intrinsic, the observational uncertainties of both $E_{X,\text{iso}}$ and E_p could make such a dispersion. Figure 8 evidently shows that the $E_{\text{iso},X} - E_p - t_b$ correlation is different from the Liang-Zhang relation. This suggests that t_b and $t_{b,\text{opt}}$ may have distinct physical origins. The positive correlation between $E_{\text{iso},X}$ and t_b is consistent with energy injection origin of t_b , namely, a longer injection episode gives more energy. The negative correlation between $E_{\text{iso},\gamma}$ and $t_{b,\text{opt}}$ may step back to the standard energy reservoir argument of Frail et al. (2001), which suggests a connection between $t_{b,\text{opt}}$ and the jet opening angle of the outflow.

7. CONCLUSIONS AND DISCUSSION

We have presented a comprehensive analysis of the *Swift* XRT light curves of long GRBs, focusing on the properties of the shallow decay phase and its relation with the follow-up decay phase. Our sample includes 53 bursts whose X-ray emissions are bright enough to perform spectral and temporal analyses for both phases. We summarize our results as follows.

(1) We find that the distributions of the characteristic properties of the shallow decay phase are log-normal or normal, i.e., $\log t_b/s = 4.09 \pm 0.61$, $\log S_X/\text{erg cm}^{-2} = -6.52 \pm 0.69$, $\Gamma_{X,1} = 2.09 \pm 0.21$, and $\alpha_1 = 0.35 \pm 0.35$ (quoted errors are at 1σ confidence level).

(2) The $E_{\text{iso},X}$ of the shallow decay phase is linearly correlated with the prompt gamma-ray phase, i.e., $\log E_{X,\text{iso}} = (1.00 \pm 0.16) \log E_{\text{iso},\gamma} - (0.5 \pm 8.12)$ (with a Spearman correlation coefficient $r = 0.79$ and a chance probability $p < 10^{-4}$). The spectrum of the shallow decay phase is softer than the prompt gamma-ray phases, except for some typical XRFs.

(3) Except for GRB 061202, no spectral evolution is observed during the transition from the shallow decay to the follow-up decay phases. The post break phase in most bursts is consistent with the closure relations of the external shock models. Six out of the 13 bursts with well-sampled optical light curves show an achromatic break in both X-ray and optical bands, but the other 7 cases either

do not show any break or have a break at a different epoch in the optical band. This poses an issue to explain t_b of these bursts as the end of the energy injection phase.

(4) Four bursts (GRBs 060413, 060522, 060607A, and 070110) in our sample have a post-break phase significantly deviate from the external shock models. The decay indices are much steeper than model requirements. The optical light curves of the latter two bursts evolve distinctly from the X-ray light curves. We suggest that the X-ray and optical emissions of these bursts are from different emission sites, and the X-ray plateaus are of internal origin and demand a long-live emission component from the central engine.

(5) Within the scenario of the refreshed external shocks, the average energy injection index $q \sim 0$, suggesting a roughly constant injection luminosity from the central engine.

(6) With a sub-sample of 27 bursts with known redshifts that satisfy the closure relations of the standard external fireball models, we discover an empirical multi-variable relation among $E_{\text{iso},X}$, E_p' , and t_b' (Eq.[7]), which is distinctly different from the $E_{\text{iso},\gamma} - E_p' - t_{b,\text{opt}}'$ relation discussed by Liang & Zhang (2005).

(7) There is no significant correlation between t_b' and the other parameters $E_{\text{iso},\gamma}$ and E_p' (unlike $t_{b,\text{opt}}'$). This suggests that the apparent $E_{j,\gamma} - E_p'$ relation by assuming a jet origin of t_b (Willingale et al. 2007) is likely a manifestation of the Amati-relation.

These results suggest that the shallow decay segment observed in most bursts is consistent with having an external forward shock origin, probably due to a continuous energy injection into the forward shock from a long-lived central engine. Therefore, the scenarios that completely abandon the external shock models (e.g. Ghisellini et al. 2007; Genet et al. 2007; Uhm & Beloborodov 2007; Shao & Dai 2007) may not be demanded by the data, and these models need to explain the apparent consistency of the $\alpha - \beta$ data with the simple closure relations of the forward shock models.

Since the energy injection break is due to a hydrodynamic effect, achromatism is one of a key feature of the model. Although about half cases satisfy such a constraint, at least some X-ray breaks are chromatic (even if the post break segment is well consistent with the standard afterglow model). This poses a great issue to argue that these X-ray breaks are energy injection breaks. Invoking different emission regions (e.g. Zhang & Mészáros 2002) may solve the problem, although more detailed modelling is needed. Crossing of a cooling break would also result in a temporal break, but it would also lead to a change of the spectral index by ~ 0.5 . From Table 1 we find that the changes of the X-ray spectral indices across the break of these bursts are 0.01 ± 0.10 (050318), 0.04 ± 0.10 (050319), 0.08 ± 0.12 (050401), and 0.03 ± 0.09 (050802). These results confidently rule out such a possibility. Genet et al. (2007) account for these chromatic breaks as due to a long-live reverse shock in which only a small fraction of electrons are accelerated. The big issue of such an interpretation is how to “hide” the emission from the forward shock, which carries most of the energy.

Assuming a simple energy injection law $L(t) \propto t^{-q}$, we find that averagely speaking the injection luminosity

could be almost a constant. This places some constraints on the physical models of the energy injection models. The constant injection luminosity agree with the expectation of the energy injection model from a central pulsar (Dai & Lu 1998a; Zhang & Mészáros 2001), suggesting that the pulsar injection model may be consistent with the data at least for some GRBs (see also Grupe et al. 2007; Fan & Xu 2006; De Pasquale et al. 2007; Yu et al. 2007).

The temporal decay slopes of some bursts following the shallow decay phase are shallower than the model predictions [Fig. 5, see also Fig. 5(a) in Willingale et al. 2007]. This discrepancy may be alleviated by different ways. First, as shown in Fig. 1, α_2 could be systematically steeper if a smoother broken power law model (with smaller ω) is adopted. Second, theoretically the temporal breaks involving external shocks are usually not sharp. Other effects, such as delay of transfer of the fireball energy to the forward shock (Kobayashi & Zhang 2007), and the structured jet effect (Zhang et al. 2004; Kumar et al. 2004; Yamazaki et al. 2006) would modify the simplest closure relations to make a band rather than a line in the $\alpha - \beta$ plane.

One interesting conclusion from this study is that at least for a small fraction of bursts (e.g. GRBs 060413, 060522, 060607A, and 070110), the observed shallow decay phase is likely of internal origin. This is another component other than X-ray flares that are possibly of internal origin. Contrary to the erratic X-ray flares, this component has a smoother light curve with flickering, likely due to a steady component from the central engine. A possible energy source for such a component would be the spin energy from the central engine, and an internal dissipation of the spindown power may be the origin (e.g. Troja et al. 2007). Tapping of the

rotation energy is likely through magnetic fields, either through dipolar spindown for a central millisecond pulsar (Usov 1992; Dai & Lu 1998a,b; Zhang & Mészáros 2001) or by the Blandford-Znajek mechanism for a black hole central engine (Blandford & Znajek 1977; Mészáros & Rees 1997b; Li 2000). If one accepts that such a component is common among bursts, one can speculate that the observed early X-ray emission is the sum of different emission components. The competition among these components shapes the variety of the X-ray light curves one observes. Depending on the relative importance of the internal and external components, the shallow decay segment could be possibly dominated by either the radiation from the refreshed shocks or by the steady radiation component from the internal dissipation of the central engine. In the former scenario, the shallow decay phase transits to a normal decay phase that is consistent with the external shock models. In the later scenario, the emission level of the underlying afterglow component is weaker than that from the emission component of the central engine, so that one needs a steep dropoff from the plateau to land onto the external shock emission component.

We acknowledge the use of the public data from the Swift data archive. We appreciate valuable comments and suggestions from the anonymous referee and P. O'Brien, Z. G. Dai, X. Dai, D. M. Wei, K. Ioka, L. Nava, X. Y. Wang, X. F. Wu, F. W. Zhang. This work is supported by NASA under grants NNG06GH62G, NNG05GB67G, NNX07AJ64G, NNX07AJ66G, and the National Natural Science Foundation of China under grant No. 10463001 (EWL) and 10640420144.

REFERENCES

- Asfandyarov, I., Pozanenko, A., & Ibrahimov, M. 2006, GCN, 5434
 Barbier, L., et al. 2005, GCN 4104
 Barbier, L., et al. 2006a, GCN 4961
 Barbier, L., et al. 2006b, GCN 5091
 Barbier, L., et al. 2006c, GCN 5108
 Barbier, L., et al. 2006d, GCN 5403
 Barthelmy, S. D., et al. 2005a, GCN 3682
 Barthelmy, S. D., et al. 2005b, GCN 4077
 Barthelmy, S. D., et al. 2006a, GCN 5256
 Barthelmy, S. D., et al. 2006b, GCN 5421
 Berger, E., & Gladders, M. 2006a, GCN 5162
 Berger, E., & Gladders, M. 2006b, GCN 5170
 Berger, E., & Mulchaey, J. 2005, GCN 3122
 Berger, E., et al. 2005, GCN 3368
 Blandford, R. D., & Znajek, R. L. 1977, MNRAS, 179, 433
 Bloom, J. S., 2006, GCN 5826
 Bloom, J. S., Frail, D. A., & Sari, R. 2001, AJ, 121, 2879
 Bloom, J. S., et al. 2005, GCN 3758
 Burrows, D. N., & Racusin, J. 2007, arXiv:astro-ph/0702633
 Burrows, D. N., et al. 2004, Proc. SPIE, 5165, 201
 Burrows, D. N., et al. 2005, Science, 309, 1833
 Butler, N. R., & Kocevski, D. 2007, ApJ, in press [arXiv:astro-ph/0702638]
 Cabrera, J. I., et al. 2007, arXiv:0704.0791
 Campana, S., et al. 2006, Nature, 442, 1008
 Castro-Tirado, A. J., et al. 2006, GCN 5218
 Cenko, S. B., et al. 2005, GCN 3542
 Cenko, S. B., et al. 2006a, GCN 4592
 Cenko, S. B., et al. 2006b, GCN 5155
 Chevalier, R. A. & Li, Z.-Y. 2000, ApJ, 536, 195
 Cucchiara, A., et al. 2006a, GCN 4729
 Cucchiara, A., et al. 2006b, GCN 5052
 Cummings, J., et al. 2005a, GCN 2992
 Cummings, J., et al. 2006, GCN 5443
 Cummings, J., et al. 2007, GCN 6007
 Curran, P. A., et al. 2007, A&A, 467, 1049
 Dai, Z. G. 2004, ApJ, 606, 1000
 Dai, Z. G., & Cheng, K. S. 2001, ApJ, 558, L109
 Dai, Z. G., & Lu, T. 1998a, A&A, 333, L87
 Dai, Z. G., & Lu, T. 1998b, Physical Review Letters, 81, 4301
 Dai, Z. G., Wang, X. Y., Wu, X. F., & Zhang, B. 2006, Science, 311, 1127
 Dai, X., Halpern, J. P., Morgan, N. D., Armstrong, E., Mirabal, N., Haislip, J. B., Reichart, D. E., & Stanek, K. Z. 2007, ApJ, 658, 509
 de Pasquale, M., et al. 2006, MNRAS, 365, 1031
 de Pasquale, M., et al. 2007, MNRAS, 377, 1638
 Della Valle, M., et al. 2006, Nature, 444, 1050
 Dermer, C. D. 2007, ApJ, in press (astro-ph/0606320)
 Eichler, D., & Granot, J. 2006, ApJ, 641, L5
 Fan, Y., & Piran, T. 2006, MNRAS, 369, 197
 Fan, Y. Z., & Wei, D. M. 2005, MNRAS, 364, L42
 Fan, Y. Z. & Xu, D. 2006, MNRAS, 372, L19
 Fenimore, E., et al. 2005, GCN 4217
 Fenimore, E., et al. 2006a, GCN 5295
 Fenimore, E., et al. 2006b, GCN 5831
 Frail, D. A., et al. 2001, ApJ, 562, L55
 Fynbo, J. P. U., et al. 2005c, GCN 3176
 Fynbo, J. P. U., et al. 2005b, GCN 3749
 Fynbo, J. P. U., et al. 2005a, GCN 3136
 Fynbo, J. P. U., et al. 2006, Nature, 444, 1047
 Gal-Yam, A., et al. 2006, Nature, 444, 1053
 Gehrels, N., et al. 2004, ApJ, 611, 1005
 Gehrels, N., et al. 2006, Nature, 444, 1044
 Genet, F., Daigne, F., & Mochkovitch, R. 2007, arXiv:astro-ph/0701204

- Ghirlanda, G., Ghisellini, G., & Lazzati, D. 2004, *ApJ*, 616, 331
- Ghisellini, G., Ghirlanda, G., Nava, L., & Firmani, C. 2007, *ApJ*, 658, L75
- Golenetskii, S., et al. 2006, GCN 5446
- Gou, L. J., Dai, Z. G., Huang, Y. F., & Lu, T. 2001, *A&A*, 368, 464
- Granot, J., & Kumar, P. 2006, *MNRAS*, 366, L13
- Granot, J., Königl, A., & Piran, T. 2006, *MNRAS*, 370, 1946
- Grupe, D., et al. 2007, *ApJ*, 662, 443
- Huang, K. Y., et al. 2007, *ApJ*, 654, L25
- Hullinger, D., et al. 2005a, GCN 3364
- Hullinger, D., et al. 2005b, GCN 3856
- Hullinger, D., et al. 2006, GCN 4851
- Ioka, K., Kobayashi, S., & Zhang, B. 2005, *ApJ*, 631, 429
- Ioka, K., Toma, K., Yamazaki, R., & Nakamura, T. 2006, *A&A*, 458, 7
- Jakobsson, P., 2006d, GCN 5617
- Jakobsson, P., et al. 2006a, GCN 5298
- Jakobsson, P., et al. 2006b, GCN 5319
- Jakobsson, P., et al. 2006c, *A&A*, 460, L13
- Jakobsson, P., et al. 2006c, GCN, 5337
- Jaunsen, A. O., et al. 2007, GCN 6010
- Jin, Z. P., Yan, T., Fan, Y. Z., & Wei, D. M. 2007, *ApJ*, 656, L57
- Kelson, D. & Berger, E., 2005, GCN 3101
- King, A., O'Brien, P. T., Goad, M. R., Osborne, J., Olsson, E., & Page, K. 2005, *ApJ*, 630, L113
- Kobayashi, S., & Zhang, B. 2007, *ApJ*, 655, 973
- Krimm, H., et al. 2005b, GCN, 3134
- Krimm, J. et al. 2005a, GCN 3119
- Krimm, H., et al. 2006d, GCN 5334
- Krimm, H., et al. 2006e, GCN 6058
- Krimm, H., et al. 2006c, GCN 5153
- Krimm, H., et al. 2005c, GCN, 3105
- Kumar, P., & Panaitescu, A. 2000a, *ApJ*, 541, L9
- Kumar, P., & Panaitescu, A. 2000b, *ApJ*, 541, L51
- Granot, J., Kumar, P., & Piran, T. 2004, *Astronomical Society of the Pacific Conference Series*, 312, 373
- Lamb, D., et al. 2006, GCN 4601
- Lazzati, D., & Begelman, M. C. 2006, *ApJ*, 641, 972
- Ledoux, C., et al. 2006, GCN 5237
- Li, L.-X. 2000, *ApJ*, 540, L17
- Liang, E. W., & Zhang, B. 2005, *ApJ*, 633, 611
- Liang, E. W., et al. 2006, *ApJ*, 646, 351
- Mészáros, P., & Rees, M. J. 1997a, *ApJ*, 476, 232
- Mészáros, P., & Rees, M. J. 1997b, *ApJ*, 482, L29
- Mészáros, P., 2002, *ARA&A*, 40, 137
- Mészáros, P. 2006, *Reports of Progress in Physics*, 69, 2259
- Mangano, V., et al. 2007, *A&A* in press [arXiv:0704.2235]
- Markwardt, C., et al. 2006a, GCN 4435
- Markwardt, C., et al. 2006b, GCN 5022
- Markwardt, C., et al. 2006c, GCN 4671
- Markwardt, C., et al. 2006d, GCN 5174
- Mason, K. O., et al. 2006, *ApJ*, 639, 311
- McGowan, K., Morgan, A., Mason, K., & Kennedy, T. 2005a, GCN, 3745, 1
- McGowan, K., Band, D., Brown, P., Gronwall, C., Huckle, H., & Hancock, B. 2005b, GCN, 3739, 1
- Melandri, A., et al. 2006, GCN 4539
- Misra, K., Bhattacharya, D., Sahu, D. K., Sagar, R., Anupama, G. C., Castro-Tirado, A. J., Guziy, S. S., & Bhatt, B. C. 2007, *A&A*, 464, 903
- Molinari, E., et al. 2007, *A&A*, 469, L13
- Nava, L., Ghisellini, G., Ghirlanda, G., Cabrera, J. I., Firmani, C., & Avila-Reese, V. 2007, *MNRAS*, 377, 1464
- Nousek, J. A., et al. 2006, *ApJ*, 642, 389
- O'Brien, P. T., et al. 2006b, *ApJ*, 647, 1213
- O'Brien, P. T., Willingale, R., Osborne, J. P., & Goad, M. R. 2006a, *New Journal of Physics*, 8, 121
- Page, K. L., et al. 2007, *ApJ*, in press, [arXiv:0704.1609]
- Palmer, D. et al. 2005, GCN 3737
- Palmer, D., et al. 2006a, GCN 4476
- Palmer, D., et al. 2006b, GCN 5744
- Palmer, D., et al., 2006c, GCN 5551
- Panaitescu, A., & Mészáros, P. 1999, *ApJ*, 526, 707
- Panaitescu, A., Mészáros, P., Gehrels, N., Burrows, D., & Nousek, J. 2006a, *MNRAS*, 366, 1357
- Panaitescu, A., Mészáros, P., & Rees, M. J. 1998, *ApJ*, 503, 314
- Panaitescu, A., Mészáros, P., Burrows, D., Nousek, J., Gehrels, N., O'Brien, P., & Willingale, R. 2006b, *MNRAS*, 369, 2059
- Parsons, A., 2005a, GCN 3600
- Parsons, A., 2005b, GCN 3757
- Parsons, A., et al. 2006a, GCN 5370
- Parsons, A., et al. 2006b, GCN 4912
- Parsons, A., et al. 2006c, GCN 5053
- Parsons, A., et al. 2006d, GCN 5561
- Parsons, A., et al. 2006e, GCN 5214
- Pavlenko, E., et al. 2005, GCN, 3744
- Pavlenko, E., et al. 2006a, GCN, 5317
- Pavlenko, E., et al. 2006b, GCN, 5324
- Pe'er, A., Mészáros, P., & Rees, M. J. 2006, *ApJ*, 652, 482
- Perna, R., Armitage, P. J., & Zhang, B. 2006, *ApJ*, 636, L29
- Piran, T. 2005, *Reviews of Modern Physics*, 76, 1143
- Preece, R. D., et al. 2000, *ApJS*, 126, 19
- Price, P.A., et al. 2006, GCN 5275
- Proga, D., & Zhang, B. 2006, *MNRAS*, 370, L61
- Quimby, R., et al. 2005, GCN 4221
- Quimby, R. M., et al. 2006, *ApJ*, 640, 402
- Rees, M. J., & Mészáros, P. 1994, *ApJ*, 430, L93
- Rees, M. J., & Mészáros, P. 1998, *ApJ*, 496, L1
- Rhoads, J. E. 1997, *ApJ*, 487, L1
- Rol, E., et al. 2006, GCN 5555
- Romano, P., et al. 2006, *A&A*, 456, 917
- Rumyantsev, V., Pavlenko, E., & Pozanenko, A. 2006, GCN, 5336, 1
- Rykoff, E. S., et al. 2005, *ApJ*, 631, L121
- Rykoff, E. S., et al. 2006, *ApJ*, 638, L5
- Sakamoto, T., et al. 2005a, GCN 3173
- Sakamoto, T., et al. 2005b, GCN 3730
- Sakamoto, T., et al. 2006a, GCN 4748
- Sakamoto, T., 2006b, et al. GCN 4445
- Sakamoto, T., et al. 2006c, GCN 5349
- Sakamoto, T., et al. 2006d, GCN 5887
- Sakamoto, T., et al. 2007, *ApJ*, submitted
- Sakamoto, T., et al. 2005c, GCN 3273
- Sari, R., & Mészáros, P. 2000, *ApJ*, 535, L33
- Sari, R., Piran, T., & Narayan, R. 1998, *ApJ*, 497, L17
- Sari, R., Piran, T., & Halpern, J. P. 1999, *ApJ*, 519, L17
- Sato, G., et al. 2006, GCN 5538
- Shao, L., & Dai, Z. G. 2007, *ApJ*, 660, 1319
- Soderberg, A. M., et al. 2005, GCN 4186
- Stamatikos, M., 2006, GCN 5459
- Stamatikos, M., et al. 2006, GCN 5289
- Stanek, K. Z., et al. 2007, *ApJ*, 654, L21
- Still, M., et al. 2005, *ApJ*, 635, 1187
- Tagliaferri, G., et al. 2005, *Nature*, 436, 985
- Thoen, C. C., et al. 2006, GCN 5373
- Toma, K., Ioka, K., Yamazaki, R., & Nakamura, T. 2006, *ApJ*, 640, L139
- Troja, E., et al. 2007, *ApJ*, in press [arXiv:astro-ph/0702220]
- Tueller, J., et al. 2006a, GCN 5964
- Tueller, J., et al. 2006b, GCN 5242
- Tueller, J., et al. 2006c, GCN 5395
- Uhm, Z. L., & Beloborodov, A. M. 2007, *ApJ*, in press [arXiv:astro-ph/0701205]
- Usov, V. V. 1992, *Nature*, 357, 472
- Vaughan, S., et al. 2006, *ApJ*, 638, 920
- Vreeswijk, P., 2006, GCN 5535
- Wang, W., & Dai, Z.-G. 2001, *Chinese Physics Letter*, 18, 1153
- Watson, D., et al. 2006, *ApJ*, 652, 1011
- Wei, D. M., & Lu, T. 2000, *ApJ*, 541, 203
- Willingale, R., et al. 2007, *ApJ*, 662, 1093
- Yamazaki, R., Toma, K., Ioka, K., & Nakamura, T. 2006, *MNRAS*, 369, 311
- Yost, S. A., et al. 2007, *ApJ*, 657, 925
- Yu, Y.-W., & Dai, Z.-G. 2007, *ArXiv e-prints*, 705, arXiv:0705.1108
- Yu, Y. W., Liu, X. W., & Dai, Z. G. 2007, *ArXiv e-prints*, 706, arXiv:0706.3741
- Zhang, B. 2006, *Nature*, 444, 1010
- Zhang, B. 2007, *Chinese Journal of Astronomy and Astrophysics*, 7, 1
- Zhang, B., & Mészáros, P. 2001, *ApJ*, 552, L35
- Zhang, B., & Mészáros, P. 2002, *ApJ*, 566, 712
- Zhang, B., & Mészáros, P. 2004, *International Journal of Modern Physics A*, 19, 2385

TABLE 1
XRT OBSERVATIONS AND THE FITTING RESULTS OF OUR SAMPLE

GRB	t_1 (ks) ^a	t_2 (ks) ^a	t_b (ks) ^b	$\alpha_{X,1}$ ^b	$\alpha_{X,2}$ ^b	χ^2 (dof) ^b	S_X ^c	$\Gamma_{X,1}$ ^d	$\Gamma_{X,2}$ ^d
050128	0.25	70.72	2.76(0.62)	0.49(0.07)	1.26(0.03)	40(48)	3.70(1.07)	1.87(0.14)	1.95(0.06)
050315	5.40	450.87	224.64(38.68)	0.66(0.03)	1.90(0.28)	42(52)	10.88(2.56)	2.06(0.11)	2.18(0.08)
050318	3.34	45.19	10.64(4.97)	0.90(0.23)	1.84(0.19)	27(20)	5.92(6.32)	2.09(0.08)	2.02(0.06)
050319	6.11	84.79	11.20(13.26)	0.23(0.59)	0.99(0.25)	9(9)	1.26(1.42)	2.00(0.06)	2.04(0.07)
050401	0.14	801.04	5.86(0.78)	0.57(0.02)	1.37(0.06)	106(92)	9.32(1.31)	1.91(0.05)	1.99(0.11)
050416A	0.25	261.69	1.74(1.12)	0.43(0.12)	0.90(0.04)	36(38)	0.62(0.38)	2.18(0.31)	2.15(0.10)
050505	3.07	97.19	7.87(1.57)	0.15(0.19)	1.30(0.06)	26(45)	2.34(0.68)	2.00(0.07)	2.03(0.04)
050713B	0.79	478.50	10.80(1.59)	-0.00(0.07)	0.94(0.04)	40(63)	3.28(0.35)	1.85(0.10)	1.94(0.09)
050726	0.42	17.05	1.17(0.33)	0.08(0.33)	1.31(0.09)	13(21)	1.17(0.53)	2.25(0.07)	2.07(0.06)
050801	0.07	46.10	0.25(fixed)	0.00(fixed)	1.10(0.03)	44(45)	0.16(0.01)	1.70(0.19)	1.91(0.12)
050802	0.51	83.83	4.09(0.61)	0.32(0.10)	1.61(0.04)	58(72)	3.66(0.94)	1.91(0.06)	1.89(0.07)
050803	0.50	368.89	13.71(0.90)	0.25(0.03)	2.01(0.07)	94(57)	5.96(0.51)	1.76(0.14)	2.00(0.08)
050822	6.41	523.32	66.99(44.38)	0.60(0.10)	1.25(0.19)	29(44)	4.05(3.12)	2.29(0.13)	2.36(0.11)
051008	3.09	43.77	14.67(3.82)	0.78(0.11)	1.96(0.21)	17(19)	6.87(3.43)	2.00(0.11)	2.06(0.07)
051016B	4.78	150.47	66.40(23.09)	0.71(0.08)	1.84(0.46)	15(16)	2.18(1.10)	2.15(0.13)	2.19(0.13)
051109A	3.73	639.16	27.28(7.90)	0.79(0.07)	1.53(0.08)	39(48)	10.59(4.71)	1.91(0.07)	1.90(0.07)
060105	0.10	360.83	2.31(0.14)	0.84(0.01)	1.72(0.02)	653(754)	42.98(3.84)	2.23(0.05)	2.15(0.03)
060108	0.77	165.26	22.08(7.38)	0.26(0.09)	1.43(0.17)	7(7)	0.53(0.17)	2.17(0.32)	1.75(0.15)
060109	0.74	48.01	4.89(1.10)	-0.17(0.14)	1.32(0.09)	19(13)	0.91(0.20)	2.32(0.15)	2.34(0.14)
060124	13.30	664.01	52.65(10.33)	0.78(0.10)	1.65(0.05)	165(132)	29.65(12.09)	2.10(0.03)	2.08(0.06)
060204B	4.06	98.80	5.55(0.66)	-0.59(0.72)	1.45(0.07)	21(34)	0.87(0.36)	2.54(0.14)	2.77(0.18)
060210	3.90	861.94	24.24(5.01)	0.63(0.05)	1.38(0.05)	144(133)	10.41(2.90)	2.06(0.03)	2.12(0.09)
060306	0.25	124.39	4.67(2.91)	0.40(0.11)	1.05(0.07)	30(32)	1.58(0.98)	2.09(0.16)	2.21(0.10)
060323	0.33	16.28	1.29(0.32)	-0.11(0.23)	1.55(0.16)	4(7)	0.27(0.08)	1.99(0.16)	2.02(0.13)
060413	1.20	253.52	26.43(1.12)	0.18(0.03)	3.42(0.21)	78(71)	13.77(0.82)	1.60(0.08)	1.50(0.10)
060428A	0.23	271.10	11.04(6.58)	0.27(0.09)	0.88(0.08)	25(21)	3.79(1.74)	2.11(0.24)	2.05(0.14)
060502A	0.24	593.06	72.57(15.05)	0.53(0.03)	1.68(0.15)	11(26)	5.09(1.19)	2.20(0.12)	2.15(0.13)
060507	3.00	86.09	6.95(1.68)	-0.37(0.48)	1.25(0.09)	2(8)	0.40(0.16)	2.15(0.19)	2.13(0.12)
060510A	0.16	343.41	9.18(0.67)	0.10(0.03)	1.51(0.03)	93(142)	17.28(1.65)	1.91(0.09)	1.96(0.06)
060522	0.20	0.90	0.53(0.06)	0.14(0.36)	3.15(0.79)	11(11)	0.26(0.12)	2.03(0.16)	2.13(0.30)
060526	1.09	322.75	10.02(4.55)	0.30(0.12)	1.50(0.23)	34(48)	0.79(0.32)	2.08(0.09)	2.08(0.16)
060604	3.52	403.81	11.37(6.80)	0.19(0.48)	1.17(0.08)	34(41)	0.79(0.67)	2.44(0.15)	2.43(0.17)
060607A	1.52	39.52	12.34(0.19)	0.00(fixed)	3.35(0.09)	132(139)	8.45(0.17)	1.44(0.06)	1.64(0.05)
060614	5.03	451.71	49.84(3.62)	0.18(0.06)	1.90(0.07)	70(54)	4.35(0.49)	2.02(0.02)	1.93(0.06)
060707	5.32	813.53	22.21(54.08)	0.37(0.96)	1.09(0.17)	8(11)	0.64(2.01)	1.88(0.09)	2.06(0.20)
060708	3.81	439.09	6.66(3.84)	0.49(0.54)	1.30(0.09)	39(34)	0.96(1.06)	2.41(0.17)	2.28(0.12)
060714	0.32	331.97	3.70(0.97)	0.34(0.10)	1.27(0.05)	53(73)	1.48(0.46)	2.15(0.08)	2.04(0.11)
060719	0.28	182.15	9.57(2.70)	0.40(0.06)	1.31(0.10)	19(26)	1.30(0.37)	2.35(0.13)	2.38(0.26)
060729	0.42	2221.24	72.97(3.02)	0.21(0.01)	1.42(0.02)	459(459)	19.58(0.83)	3.35(0.04)	2.26(0.05)
060804	0.18	122.07	0.86(0.22)	-0.09(0.15)	1.12(0.07)	18(24)	0.97(0.18)	2.04(0.23)	2.14(0.15)
060805A	0.23	75.91	1.30(0.70)	-0.17(0.41)	0.97(0.13)	11(17)	0.06(0.03)	2.10(0.10)	1.97(0.37)
060807	0.28	166.22	8.04(0.35)	0.06(0.03)	1.73(0.05)	67(36)*	1.94(0.11)	2.30(0.28)	2.22(0.08)
060813	0.09	74.25	1.77(0.27)	0.55(0.03)	1.25(0.03)	86(75)	7.31(1.36)	2.09(0.16)	2.04(0.04)
060814	0.57	399.37	17.45(1.71)	0.54(0.02)	1.59(0.05)	81(57)	6.93(0.87)	2.11(0.09)	2.30(0.05)
060906	1.32	36.69	13.66(3.29)	0.35(0.10)	1.97(0.36)	3(7)	0.96(0.29)	2.28(0.37)	2.12(0.17)
060908	0.08	363.07	0.95(0.34)	0.70(0.07)	1.49(0.09)	98(59)*	1.28(0.61)	2.41(0.21)	2.00(0.08)
060912	0.42	86.80	1.13(0.31)	0.13(0.30)	1.19(0.08)	8(26)	0.37(0.15)	2.08(0.11)	1.95(0.13)
061021	0.30	594.16	9.59(2.17)	0.52(0.03)	1.08(0.03)	94(87)	3.59(0.87)	1.81(0.04)	1.70(0.13)
061121	4.89	353.10	24.32(4.38)	0.75(0.06)	1.63(0.05)	121(147)	19.89(6.14)	2.00(0.04)	1.93(0.05)
061202	0.93	357.04	41.65(5.36)	0.10(0.04)	2.20(0.18)	55(49)	13.80(1.12)	2.15(0.09)	3.55(0.44)
061222A	22.78	724.64	32.73(2.17)	-0.61(0.45)	1.75(0.04)	102(59)*	6.62(1.89)	2.46(0.07)	2.22(0.12)
070110	4.10	28.72	20.40(0.44)	0.11(0.05)	8.70(0.88)	43(66)	3.59(0.23)	2.16(0.11)	2.21(0.09)
070129	1.32	546.36	20.12(3.14)	0.15(0.07)	1.31(0.06)	42(70)	1.47(0.24)	2.25(0.07)	2.30(0.10)

^aThe starting and ending time of our lightcurve fitting

^bThe break time and the decay slopes before and after the break, and the fitting χ^2 (degrees of freedom).

^cThe X-ray fluence (in units of 10^{-7} erg cm^{-2}) of the shallow decay phase calculated by integrating the fitting light curve from 10 seconds post the GRB trigger to t_b .

^dThe X-ray photon indices before and after t_b .

* The fitting results of these bursts have an unaccepted reduced χ^2 due to significant flicking.

Zhang, B., Dai, X., Lloyd-Ronning, N. M., & Mészáros, P. 2004, ApJ, 601, L119

Zhang, B., Fan, Y. Z., Dyks, J., Kobayashi, S., Mészáros, P., Burrows, D. N., Nousek, J. A., & Gehrels, N. 2006, ApJ, 642, 354

Zhang, B., Liang, E.-W., Page, K., Grupe, D., et al. 2007a, ApJ, 655, 989

Zhang, B., Zhang, B.-B., Liang, E.-W., Gehrels, N., Burrows, D. N., & Mészáros, P. 2007b, ApJ, 655, L25

Zhang, B.-B., Liang, E.-W., & Zhang, B. 2007, ApJ, in press (astro-ph/0612246) (Paper I)

TABLE 2
 BAT OBSERVATIONS AND REDSHIFTS OF OUR SAMPLE

GRB	$T_{90}(s)$	S_{γ}^a	$\Gamma_{\gamma,1}^b$	$\Gamma_{\gamma,2}^b$	$E_p(\text{keV})^b$	ref _{BAT} ^c	z	ref _z ^c
050128	13.8(2.0)	45.00(5.00)	1.50(0.05)		133.1(30.2)	2992		
050315	96.0(10.0)	28.00(3.00)	1.28(0.00)	2.20	37.0(8.0)	3105	1.95	3101
050318	32.0(2.0)	21.00(2.00)	2.10(0.11)		39.5(12.4)	3134	1.44	3122
050319	10.0(2.0)	8.00(0.80)	1.25(0.00)	2.15	28.0(6.0)	3119, Z07	3.24	3136
050401	33.0(2.0)	140.00(14.00)	1.15(0.00)	2.65	132.0(16.0)	3173, Z07	2.90	3176
050416A	2.4(0.2)	3.80(0.40)	1.00(0.00)	3.22	16.0(3.0)	3273	0.65	3542
050505	60.0(2.0)	41.00(4.00)	1.50(0.10)		133.1(41.0)	3364, Z07	4.27	3368
050713B	75.0(7.5)	82.00(10.00)	1.00(0.13)		109.0(32.0)	3600, Z07		
050726	30.0(3.0)	43.00(7.00)	1.00(0.16)		984.0(200.0)	3682, Z07		
050801	20.0(3.0)	4.40(1.00)	1.40(0.00)	2.00	33.0(7.0)	3730, Z07		
050802	13.0(2.0)	28.00(3.00)	1.12(0.00)	2.48	118.0(77.0)	3737, Z07	1.71	3749
050803	110.0(11.0)	39.00(3.00)	1.05(0.10)		150.0(68.0)	3757, Z07	0.42	3758
050822	102.0(2.0)	34.00(3.00)	1.00(0.00)	2.48	36.0(7.0)	3856		
051008	280.0(28.0)	540.00(10.00)	0.98(0.09)		865.0(178.0)	4077, Z07		
051016B	4.0(0.1)	1.70(0.20)	2.38(0.23)		25.2(11.2)	4104	0.94	4186
051109A	36.0(2.0)	21.00(3.00)	1.50(0.20)		133.1(69.0)	4217	2.35	4221
060105	55.0(5.0)	182.00(4.00)	1.11(0.03)		394.8(75.2)	4435		
060108	14.4(1.0)	3.70(0.40)	2.01(0.17)		46.3(18.1)	4445	2.03	4539
060109	116.0(3.0)	6.40(1.00)	1.96(0.25)		50.7(26.3)	4476		
060124	800.0(10.0)	110.00(10.00)	1.17(0.27)		326.5(277.3)	4601	2.30	4592
060204B	134.0(5.0)	30.00(2.00)	0.82(0.40)		96.8(41.0)	4671		
060210	255.0(10.0)	77.00(4.00)	1.52(0.09)		126.9(36.7)	4748	3.91	4729
060306	61.0(2.0)	22.00(1.00)	1.85(0.10)		62.4(18.7)	4851		
060323	18.0(2.0)	5.70(0.60)	1.53(0.17)		124.0(55.3)	4912		
060413	150.0(10.0)	36.00(1.00)	1.67(0.08)		90.4(24.5)	4961		
060428A	39.4(2.0)	14.00(1.00)	2.04(0.11)		43.9(13.8)	5022		
060502A	33.0(5.0)	22.00(1.00)	1.43(0.08)		158.2(43.4)	5053	1.51	5052
060507	185.0(5.0)	45.00(2.00)	1.83(0.10)		64.9(19.3)	5091		
060510A	21.0(3.0)	98.00(5.00)	1.55(0.10)		118.3(36.1)	5108		
060522	69.0(5.0)	11.00(1.00)	1.59(0.15)		107.9(42.7)	5153	5.11	5155
060526	13.8(2.0)	4.90(0.60)	1.66(0.20)		92.3(44.5)	5174	3.21	5170
060604	10.0(3.0)	1.30(0.30)	1.90(0.41)		56.7(46.1)	5214	2.68	5218
060607A	100.0(5.0)	26.00(1.00)	1.45(0.07)		150.5(38.6)	5242	3.08	5237
060614	102.0(5.0)	217.00(4.00)	2.13(0.04)		37.5(9.9)	5256	0.125	5275
060707	68.0(5.0)	17.00(2.00)	0.66(0.63)		66.0(25.0)	5289	3.43	5298
060708	9.8(1.0)	5.00(0.40)	1.68(0.12)		88.4(29.4)	5395		
060714	115.0(5.0)	30.00(2.00)	1.99(0.10)		48.0(14.5)	5334	2.71	J06
060719	55.0(5.0)	16.00(1.00)	2.00(0.11)		47.1(14.7)	5349		
060729	116.0(10.0)	27.00(2.00)	1.86(0.14)		61.2(21.7)	5370	0.54	5373
060804	16.0(2.0)	5.10(0.90)	1.78(0.28)		71.8(43.7)	5395		
060805A	5.4(0.5)	0.74(0.20)	2.23(0.42)		31.8(23.2)	5421		
060807	34.0(4.0)	7.30(0.90)	1.57(0.20)		112.9(56.6)	5403		
060813	14.9(0.5)	55.00(1.00)	0.53(0.15)		192.0(19.0)	5443,5446		
060814	146.0(10.0)	150.00(2.00)	1.56(0.03)		115.6(24.3)	5459		
060906	43.6(1.0)	22.10(1.40)	2.02(0.11)		45.5(14.2)	5538	3.68	5535
060908	19.3(0.3)	29.00(1.00)	1.33(0.07)		205.5(53.4)	5551	2.43	5555
060912	5.0(0.5)	13.00(1.00)	1.74(0.09)		77.9(22.3)	5561	0.94	5617
061021	46.0(1.0)	30.00(1.00)	1.31(0.06)		217.1(52.4)	5744		
061121	81.0(5.0)	137.00(2.00)	1.41(0.03)		166.5(33.2)	5831	1.31	5826
061202	91.0(5.0)	35.00(1.00)	1.63(0.07)		98.6(25.4)	5887		
061222A	72.0(3.0)	83.00(2.00)	1.39(0.04)		175.3(36.8)	5964		
070110	85.0(5.0)	16.00(1.00)	1.57(0.12)		112.9(38.4)	6007	2.35	6010
070129	460.0(20.0)	31.00(3.00)	2.05(0.16)		43.1(16.1)	6058		

REFERENCES. — J06: Jakobsson et al. 2006(c); Z07: Zhang et al. 2007a; 2992: Cummings et al. (2005); 3101: Kelson and Berger (2005); 3105: Krimm et al. (2005c); 3119: Krimm et al. (2005a); 3122: Berger and Mulchaey (2005); 3134: Krimm et al. (2005b); 3136: Fynbo et al. (2005a); 3173: Sakamoto et al. (2005a); 3176: Fynbo et al. (2005c); 3273: Sakamoto et al. (2005c); 3364: Hullinger et al. (2005a); 3368: Berger et al. (2005b); 3542: Cenko et al. (2005); 3600: Parsons et al. (2005a); 3682: Barthelmy et al. (2005a); 3730: Sakamoto et al. (2005b); 3737: Palmer et al. (2005); 3749: Fynbo et al. (2005b); 3757: Parsons (2005b); 3758: Bloom et al. (2005); 4217: Fenimore et al. (2005); 4221: Quimby et al. (2005); 4435: Markwardt et al. (2006a); 4445: Sakamoto et al. (2006b); 4476: Palmer et al. (2006a); 4539: Melandri et al. (2006); 4592: Cenko et al. (2006a); 4601: Lamb et al. (2006); 4671: Markwardt et al. (2006c); 4729: Cucchiara et al. (2006a); 4748: Sakamoto et al. (2006a); 4851: Hullinger et al. (2006); 4912: Parsons et al. (2006b); 4961: Barbier et al. (2006a); 5022: Markwardt et al. (2006b); 5052: Cucchiara et al. (2006b); 5053: Parsons et al. (2006c); 5091: Barbier et al. (2006b); 5108: Barbier et al. (2006c); 5153: Krimm et al. (2006c); 5155: Cenko et al. (2006a); 5162: Berger and Gladders (2006a); 5170: Berger and Gladders (2006b); 5174: Markwardt et al. (2006d); 5214: Parsons et al. (2006e); 5218: Castro-Tirado et al. (2006); 5237: Ledoux et al. (2006); 5242: Tueller et al. (2006b); 5256: Barthelmy, S. et al. (2006a); 5275: Price et al. (2006); 5289: Stamatikos et al. (2006b); 5295: Fenimore et al. (2006a); 5298: Jakobsson et al. (2006a); 5320: Jakobsson et al. (2006c); 5334: Krimm et al. (2006d); 5349: Sakamoto et al. (2006c); 5370: Parsons et al. (2006a); 5373: Thoene et al. (2006); 5395: Tueller et al. (2006c); 5403: Barbier et al. (2006d); 5421: Barthelmy et al. (2006b); 5443: Cummings et al. (2006); 5446: Golenetskii et al. (2006); 5459: Stamatikos et al. (2006a); 5535: Vreeswijk (2006); 5538: Sato et al. (2006); 5551: Palmer et al. (2006c); 5555: Rol et al. (2006); 5561: Parsons et al. (2006d); 5617: Jakobsson (2006d); 5744: Palmer et al. (2006b); 5826: Bloom (2006); 5831: Fenimore et al. (2006b); 5887: Sakamoto et al. (2006d); 5964: Tueller et al. (2006a); 6007: Cummings et al. (2007); 6010: Jaunsen et al. (2007); 6058: Krimm et al. (2006e).

^a The observed gamma-ray fluence and its error in 15–150 keV band, in units of 10^{-7} erg cm^{-2} .

^b The spectrum of the prompt gamma-rays is generally fitted by a simple power-law, $f_{\nu} \propto \nu^{-\Gamma_{\gamma,1}}$. We estimate the E_p for these bursts with the empirical relation between $\Gamma_{\gamma,1}$ and E_p for the BAT observations. Few cases are fitted with a cut-off power-law or the Band function (the photon indices before and after the break energy is $\Gamma_{\gamma,1}$ and $\Gamma_{\gamma,2}$, respectively).

^c References for BAT data and redshift data.

TABLE 3
THE OPTICAL OBSERVATIONS AND OUR FITTING RESULTS

GRB	t_1 (ks) ^a	t_2 (ks) ^a	$t_{b,O}$ (ks) ^b	$\alpha_{O,1}$ ^b	$\alpha_{O,2}$ ^b	$\chi^2/(\text{dof})$ ^b	ref
050318	3.23	22.83	-	0.84(0.22)	-	0.5(1)	(1)
050319	2.00	204.74	-	0.42(0.02)	-	11(16)	(2)-(4)
050401	0.06	1231.18	-	0.80(0.01)	-	43(12)	(5)-(7)
050801	0.02	9.49	0.19(0.02)	-0.02(0.07)	1.10(0.02)	26(42)	(8)
050802	0.34	127.68	-	0.85(0.02)	-	50(10)	(9)-(11)
051109A	0.04	20170.00	21.80(10.95)	0.66(0.02)	1.10(0.08)	106(42)	(12)
060124	3.34	1979.30	-	0.85(0.02)	-	11(19)	(13)-(14)
060210	0.09	7.19	0.70(0.18)	0.01(0.24)	1.23(0.08)	5(12)	(15)-(16)
060526	0.06	893.55	84.45(5.88)	0.67(0.02)	1.80(0.04)	116(56)	(17)
060607A	0.07	13.73	0.16(fixed)	-3.07(0.25)	1.18(0.02)	92(35)	(18)
060614	1.54	934.36	39.09(1.71)	-0.40(0.05)	2.16(0.03)	114(24)	(19)-(21)
060714	3.86	285.87	1.00	0.01(fixed)	1.41(0.03)	35(11)	(22)-(26)
060729	20.00	662.39	43.29(5.15)	-0.37(0.34)	1.34(0.06)	36(27)	(27)
061121	0.26	334.65	1.70(0.73)	0.17(fixed)	0.99(0.05)	18(23)	(28)
070110	0.66	34.76	-	0.43(0.08)	-	1(4)	29

REFERENCES. — (1)Still et al. (2005); (2) Quimby et al. (2006); (3) Huang et al. (2007); (4) Mason et al. (2006); (5) De Pasquale (2006); (6) Rykoff et al. (2005); (7) Watson et al. (2006); (8) Rykoff et al. (2006); (9) McGowan et al.(2005a); (10)Pavlenko et al.(2005); (11) McGowan et al.(2005b);(12) Yost et al. (2007); (13) Misra et al. (2007); (14) Romano et al. 2006; (15) Curran et al.(2007);(16) Stanek et al.(2007); (17) Dai et al. 2007; (18) Molinari et al.(2007); (19)Fynbo et al.(2006); (20)Della Valle et al.(2006); (21)Gal-Yam et al.(2006); (22) Asfandyarov et al.(2006); (23)Rumyantsev et al.(2006); (24) Pavlenko et al.(2006a); (25) Jakobsson et al.(2006c); (26)Pavlenko et al.(2006b); (27) Grupe et al.(2007); (28) Page et al.(2007); (29) Troja et al.(2007).

^aThe time interval concerned in our fitting

^bFor a smooth broken power law fit, $t_{b,O}$, $\alpha_{O,1}$, $\alpha_{O,2}$ are the break time and the decay slopes before and after the break. For a simple power law fit, the decay index and its error are shown in column $\alpha_{O,1}$. In order to make the fittings more reasonable, we assume an error of 0.1 mag for those data points without observational error available.

TABLE 4
REST-FRAME PROPERTIES OF THE BURSTS WITH KNOWN REDSHIFTS IN OUR SAMPLE

GRB	$\log T'_{90}$ (s)	$\log E'_p$ (keV)	$\log E_{\text{iso},\gamma}$ (erg)	$\log E_{\text{iso},\gamma}^p$ (erg)	$\log E_{\text{iso},X}$ (erg)	$\log t'_b$ (s)
050315	1.51(0.05)	2.0(0.1)	52.41(0.05)	52.84	51.94(0.10)	4.83(0.07)
050318	1.12(0.03)	2.0(0.1)	52.04(0.04)	52.38	51.88(0.46)	4.03(0.20)
050319	0.37(0.09)	2.1(0.1)	52.24(0.04)	52.69	52.03(0.49)	4.01(0.51)
050401	0.93(0.03)	2.7(0.1)	53.41(0.04)	53.69	52.82(0.06)	3.77(0.06)
050416A	0.16(0.04)	1.4(0.1)	50.62(0.05)	51.00	49.69(0.26)	2.88(0.28)
050505	1.06(0.01)	2.8(0.1)	53.14(0.04)	53.51	52.62(0.13)	3.90(0.09)
050802	0.68(0.07)	2.5(0.3)	52.31(0.05)	52.62	51.86(0.11)	3.61(0.06)
050803	1.89(0.04)	2.3(0.2)	51.24(0.03)	51.67	50.29(0.04)	3.85(0.03)
051016B	0.32(0.01)	1.7(0.2)	50.59(0.05)	50.95	50.99(0.22)	4.82(0.15)
051109A	1.03(0.02)	2.6(0.2)	52.43(0.06)	52.82	52.65(0.19)	4.44(0.13)
060108	0.68(0.03)	2.1(0.2)	51.56(0.05)	51.89	51.20(0.14)	4.34(0.15)
060124	2.38(0.01)	3.0(0.4)	53.13(0.04)	53.72	53.08(0.18)	4.72(0.09)
060210	1.72(0.02)	2.8(0.1)	53.36(0.02)	53.72	53.18(0.12)	4.38(0.09)
060502A	1.12(0.07)	2.6(0.1)	52.10(0.02)	52.54	51.82(0.10)	4.81(0.09)
060522	1.05(0.03)	2.8(0.2)	52.69(0.04)	53.03	51.29(0.19)	2.16(0.05)
060526	0.52(0.06)	2.6(0.2)	52.02(0.05)	52.36	51.21(0.26)	3.38(0.25)
060604	0.43(0.13)	2.3(0.4)	51.32(0.10)	51.64	50.88(0.37)	3.27(0.26)
060607A	1.39(0.02)	2.8(0.1)	52.72(0.02)	53.12	52.84(0.01)	4.09(0.01)
060614	1.96(0.02)	1.6(0.1)	50.90(0.01)	51.24	49.25(0.05)	4.70(0.03)
060707	1.19(0.03)	2.5(0.2)	52.61(0.05)	52.98	51.44(1.36)	3.95(1.06)
060714	1.49(0.02)	2.3(0.1)	52.69(0.03)	53.01	51.95(0.14)	3.57(0.11)
060729	1.88(0.04)	2.0(0.2)	51.31(0.03)	51.65	51.35(0.02)	4.86(0.02)
060906	0.97(0.01)	2.3(0.1)	52.78(0.03)	53.09	51.57(0.13)	3.62(0.10)
060908	0.75(0.01)	2.8(0.1)	52.59(0.01)	53.07	51.12(0.21)	2.32(0.16)
060912	0.41(0.04)	2.2(0.1)	51.47(0.03)	51.83	50.21(0.17)	3.05(0.12)
061121	1.54(0.03)	2.6(0.1)	52.78(0.01)	53.23	51.83(0.13)	3.90(0.08)
070110	1.40(0.03)	2.6(0.1)	52.31(0.03)	52.68	52.19(0.03)	4.31(0.01)

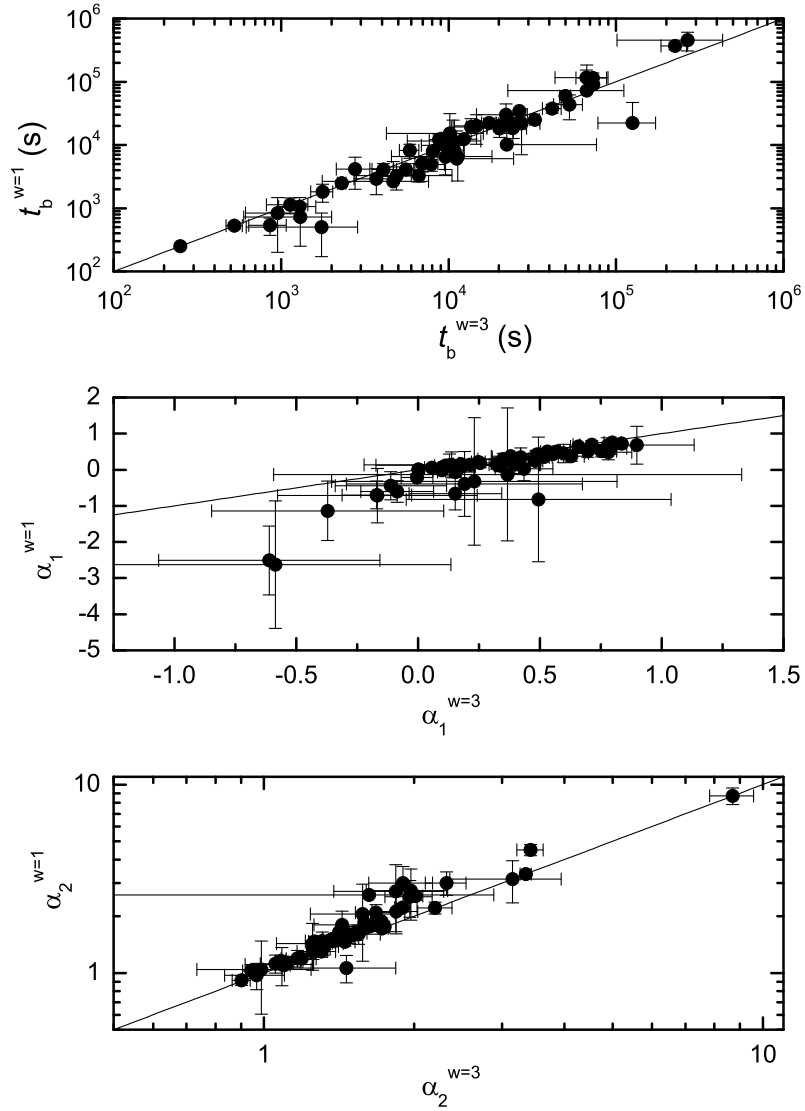


FIG. 1.— Comparison of the fitting results of smooth broken power law models with different sharpness parameters: $\omega = 1$ and $\omega = 3$. The solid lines stand for the equality of the two quantities.

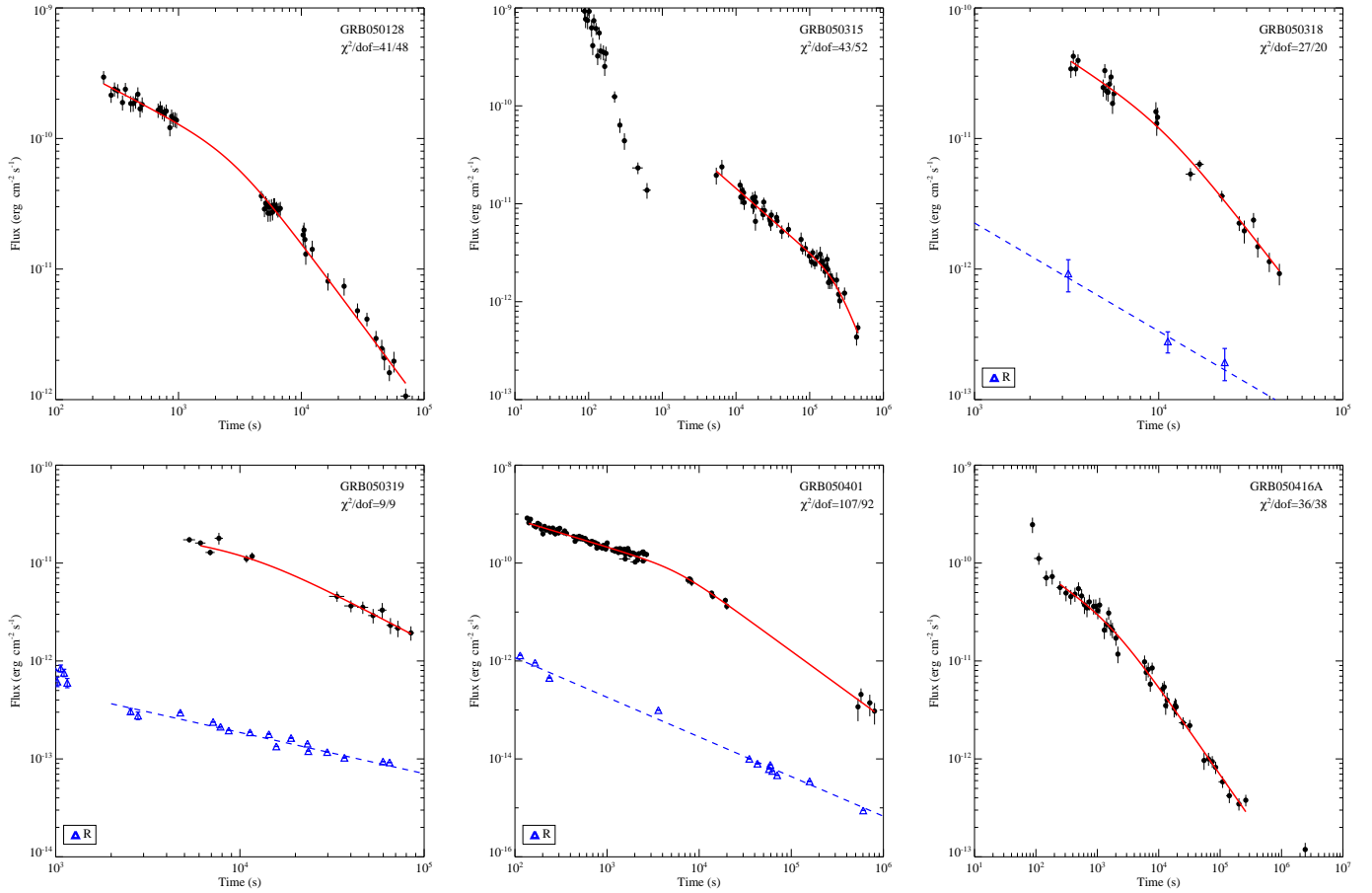


Fig.2 (continued)

FIG. 2.— The XRT light curves (dots) for the bursts in our sample. The *solid* lines are the best fits with the smooth broken power law for the shallow decay phase and its follow-up decay phase (usually the “normal” decay phase). The fitting χ^2 and degrees of freedom are shown in each plot. The optical light curves are shown by opened triangles, if they are available. They are fitted by a smooth broken power law or a simple power law as displayed by dashed lines.

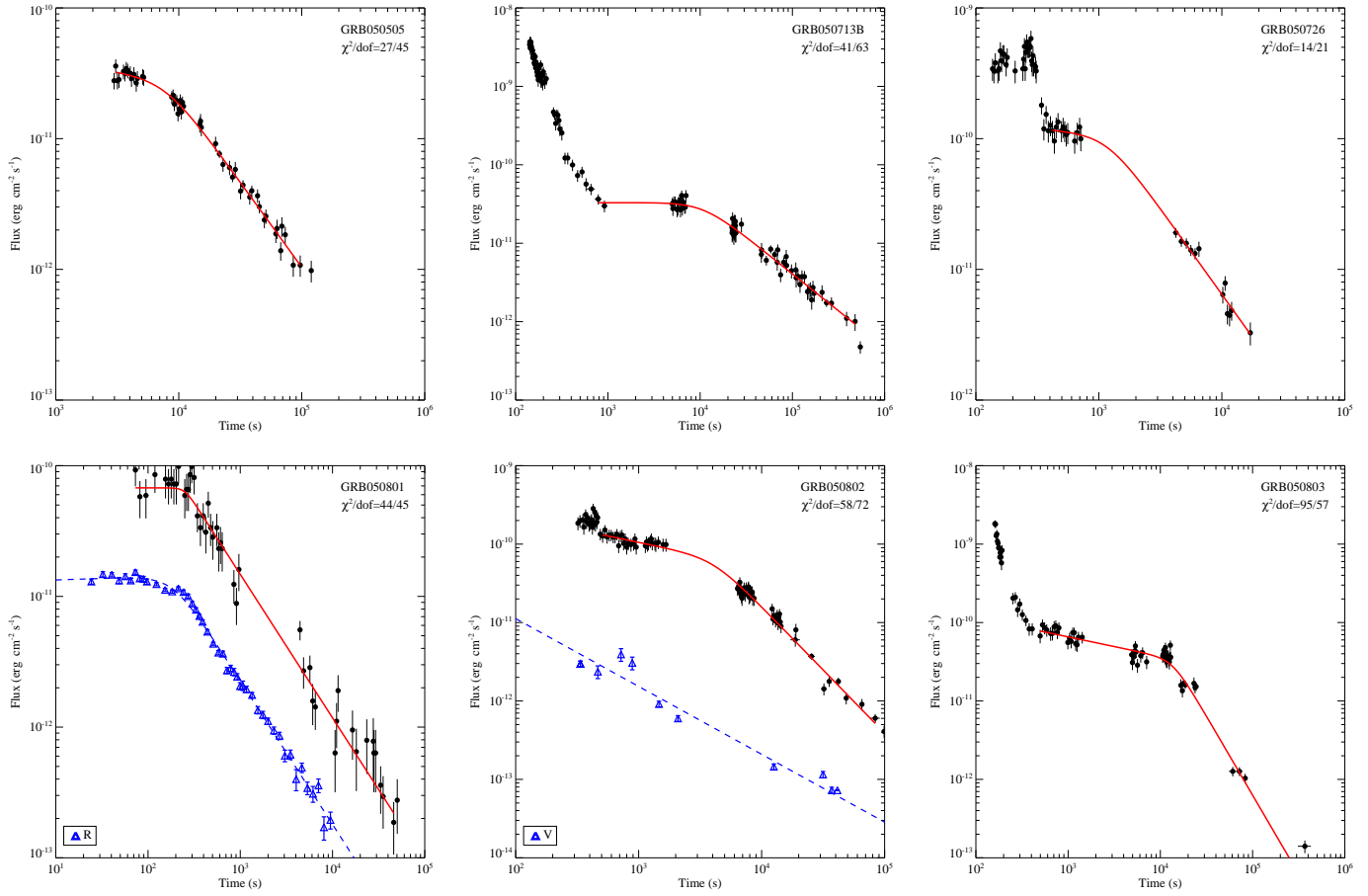


Fig.2 (continued)

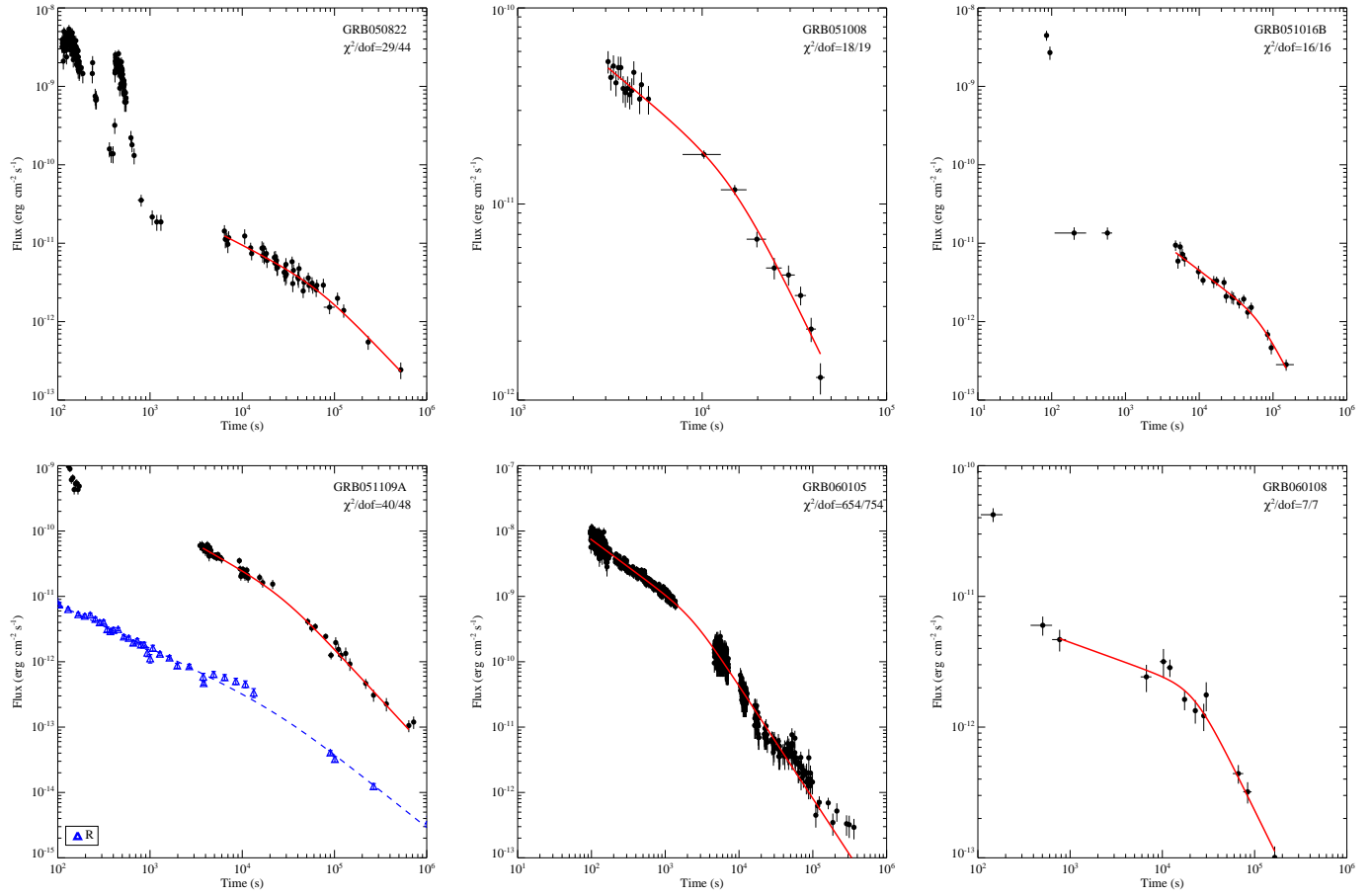


Fig.2 (continued)

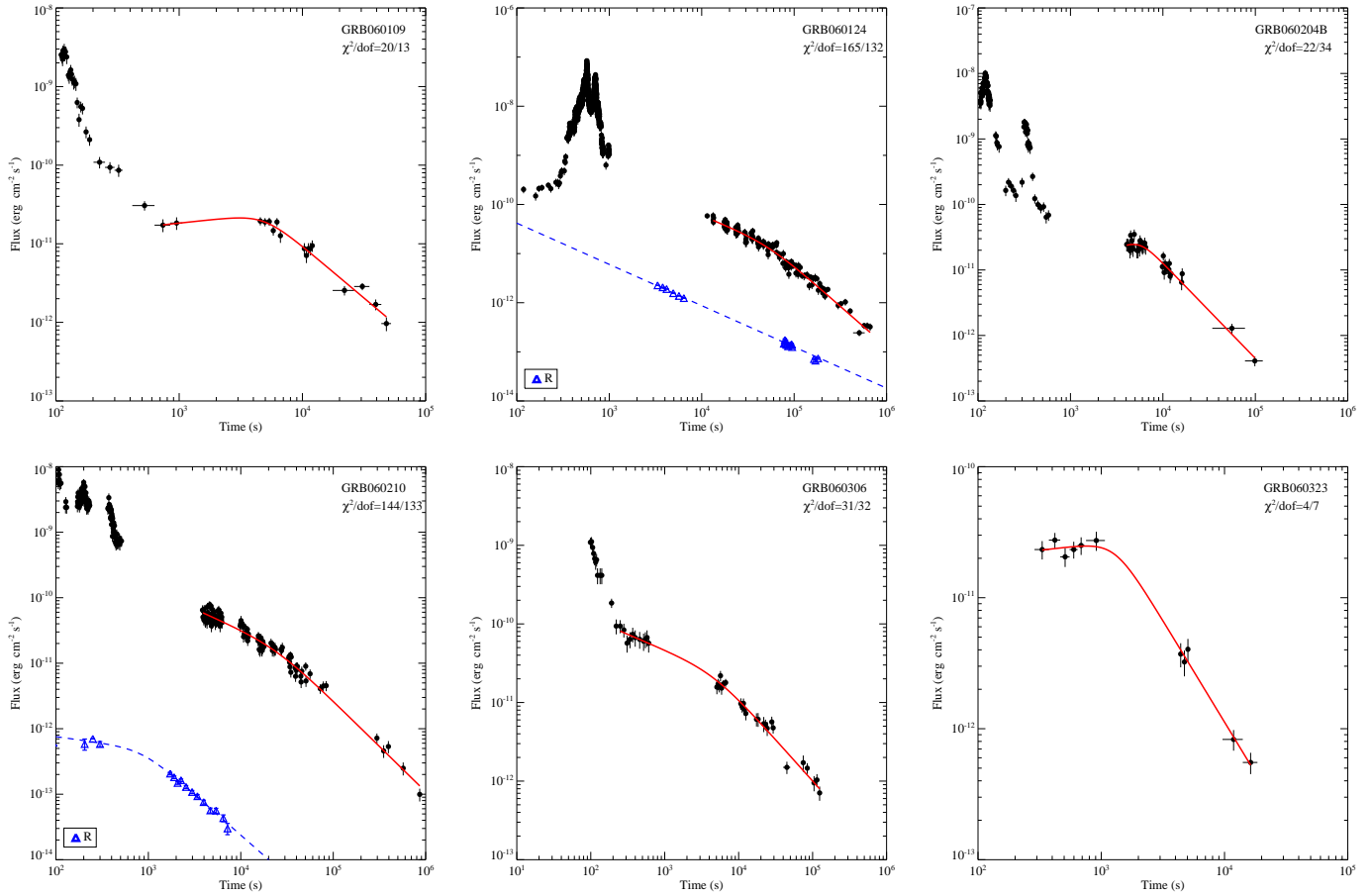


Fig.2 (continued)

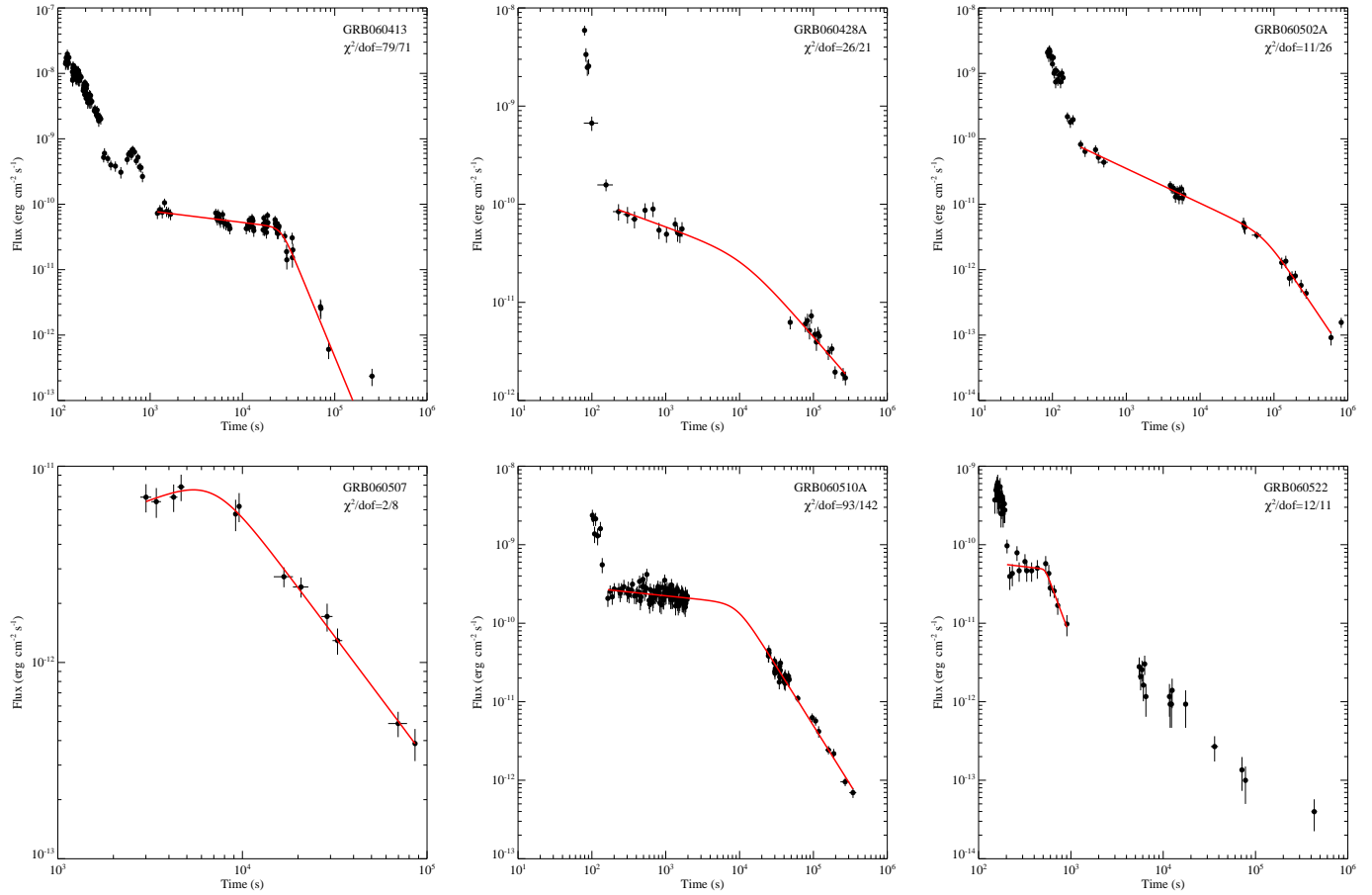


Fig.2 (continued)

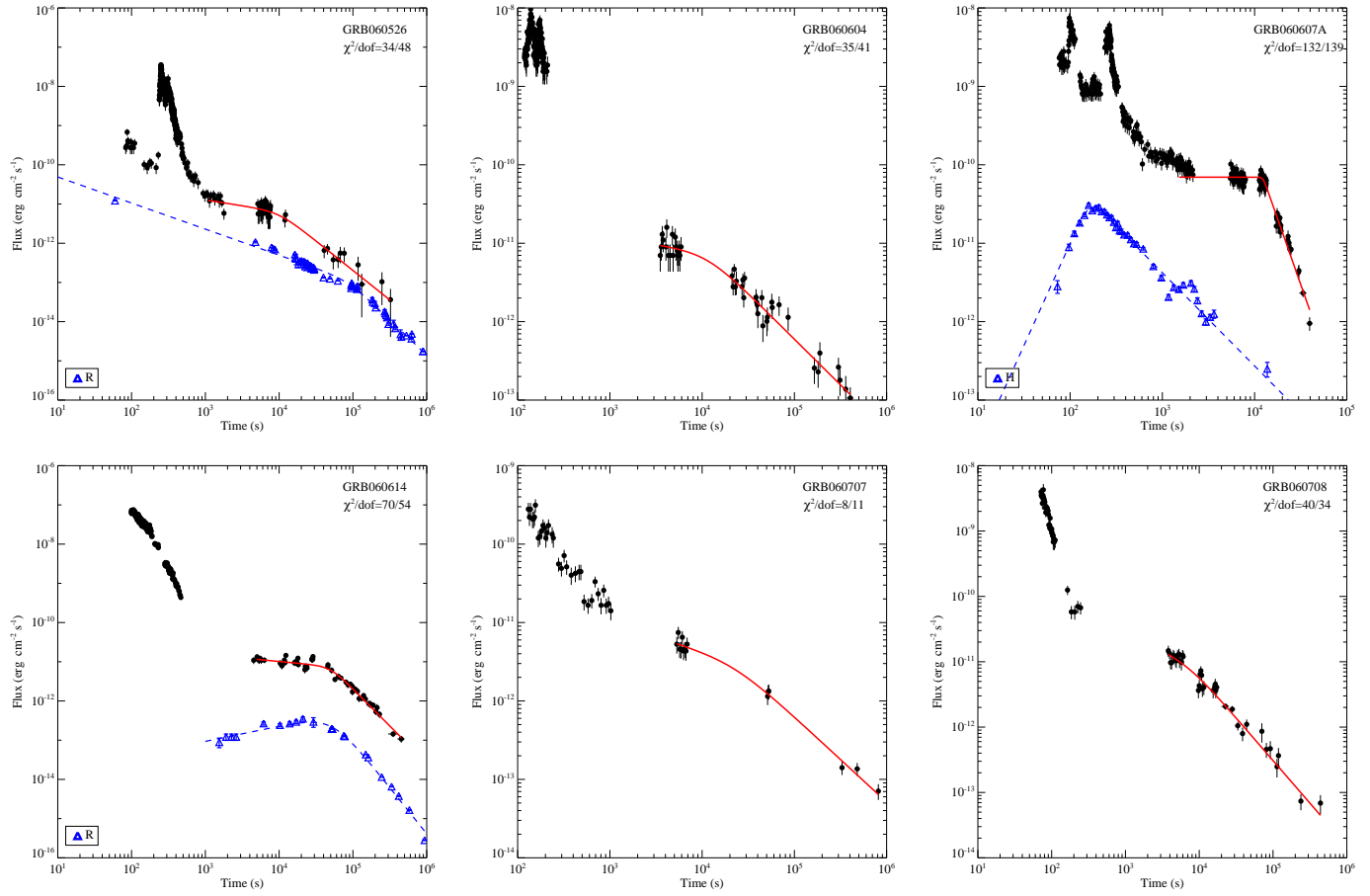


Fig.2 (continued)

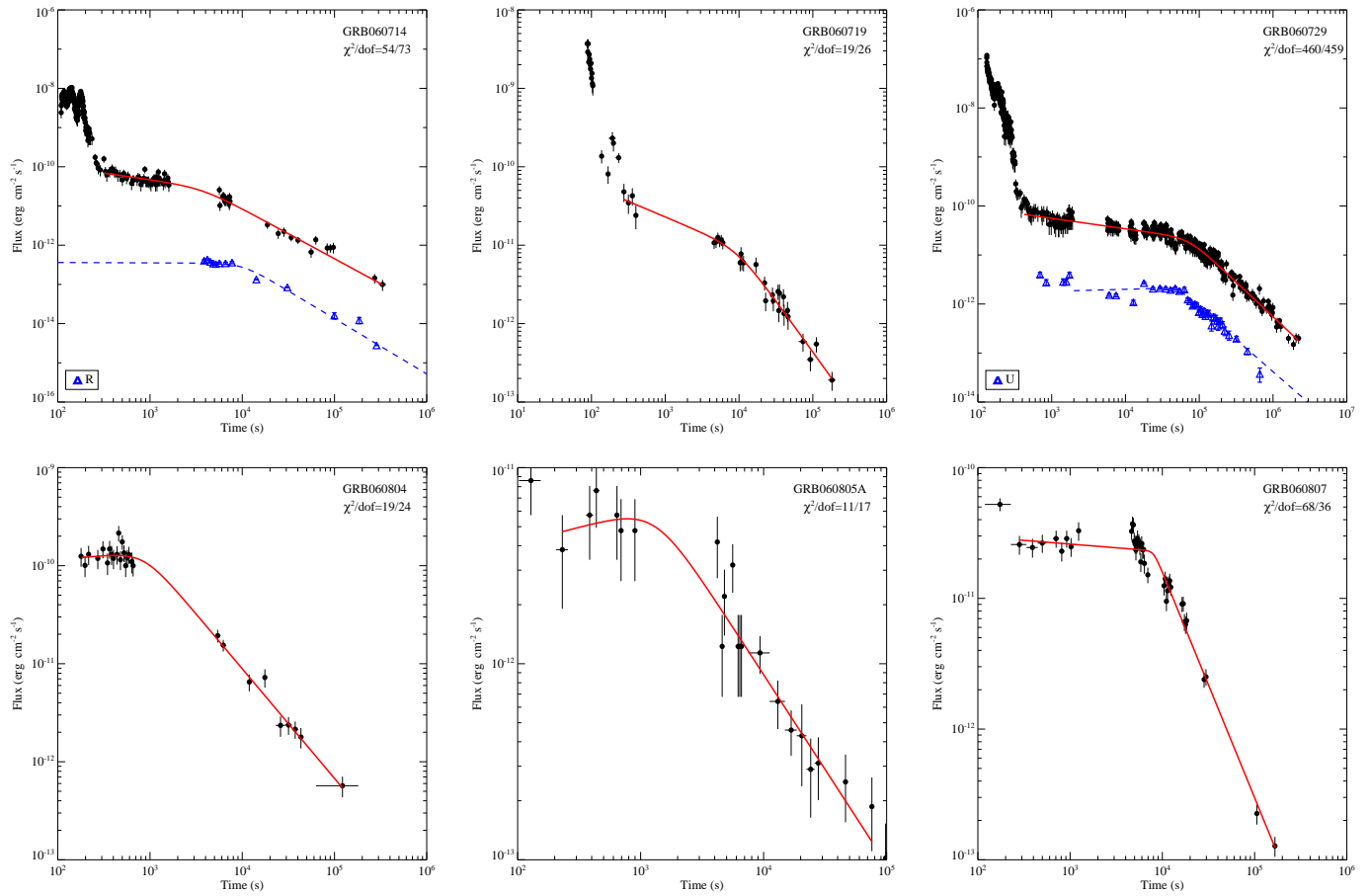


Fig.2 (continued)

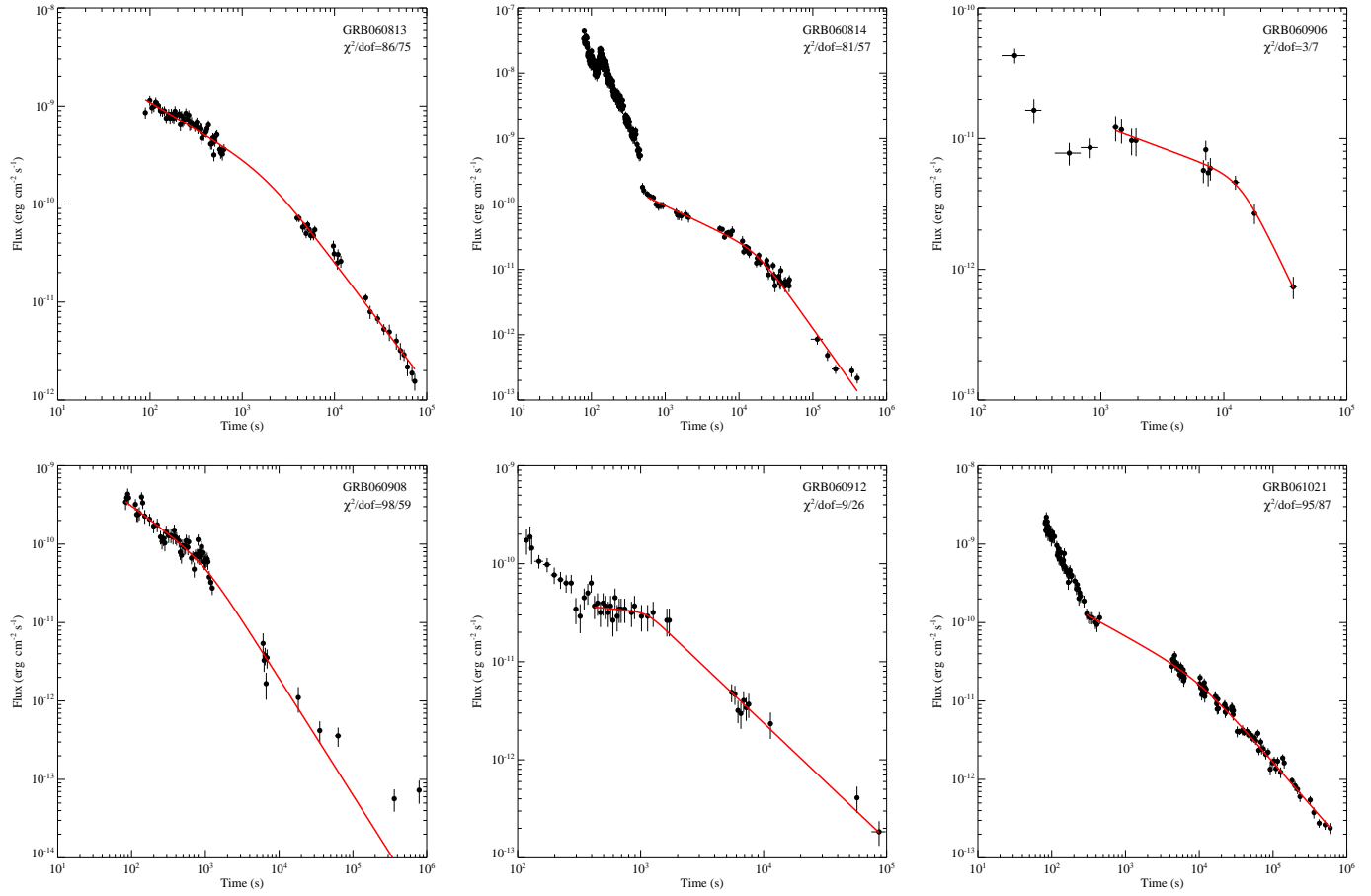


Fig.2 (continued)

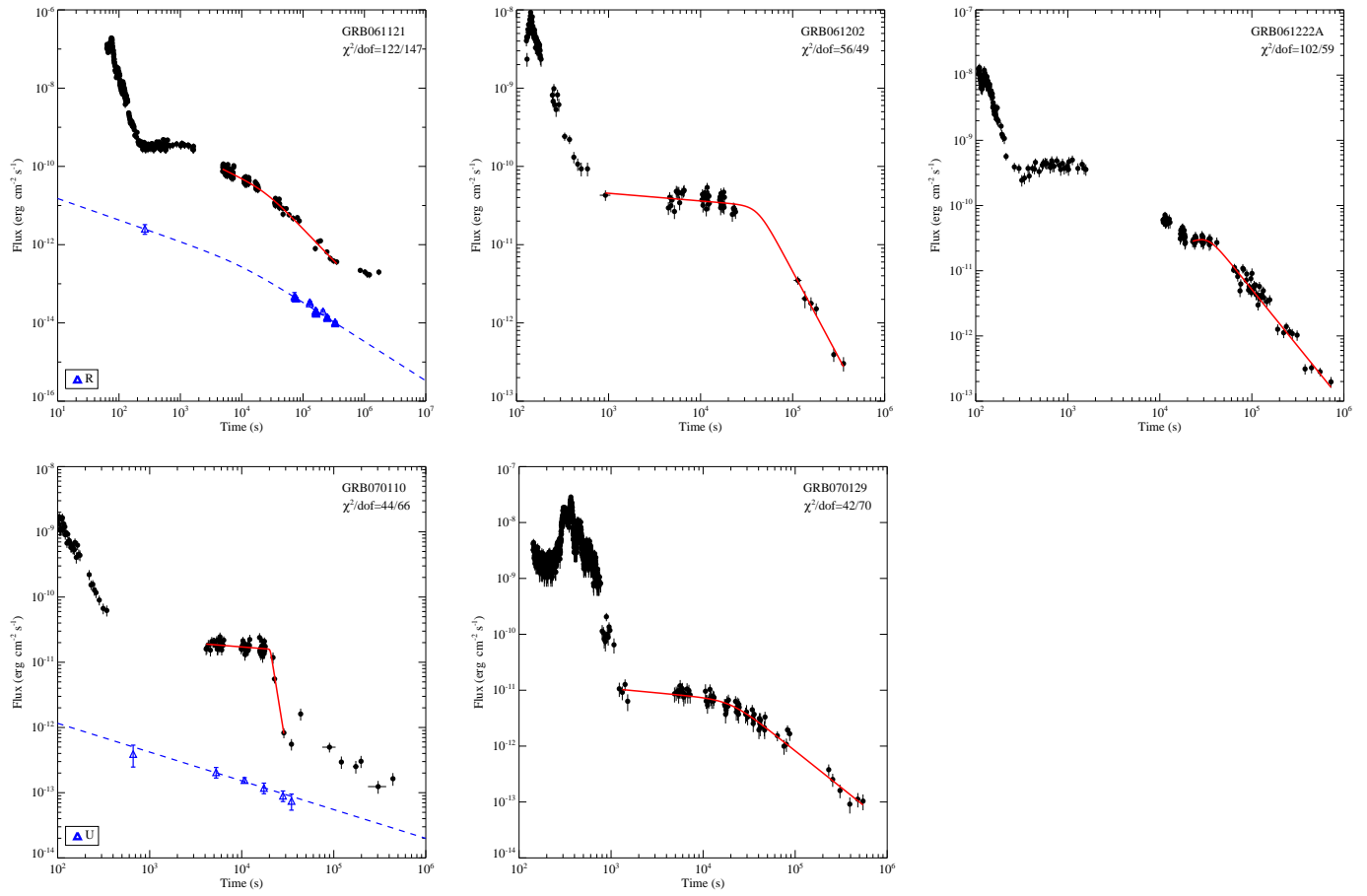


Fig.2 (continued)

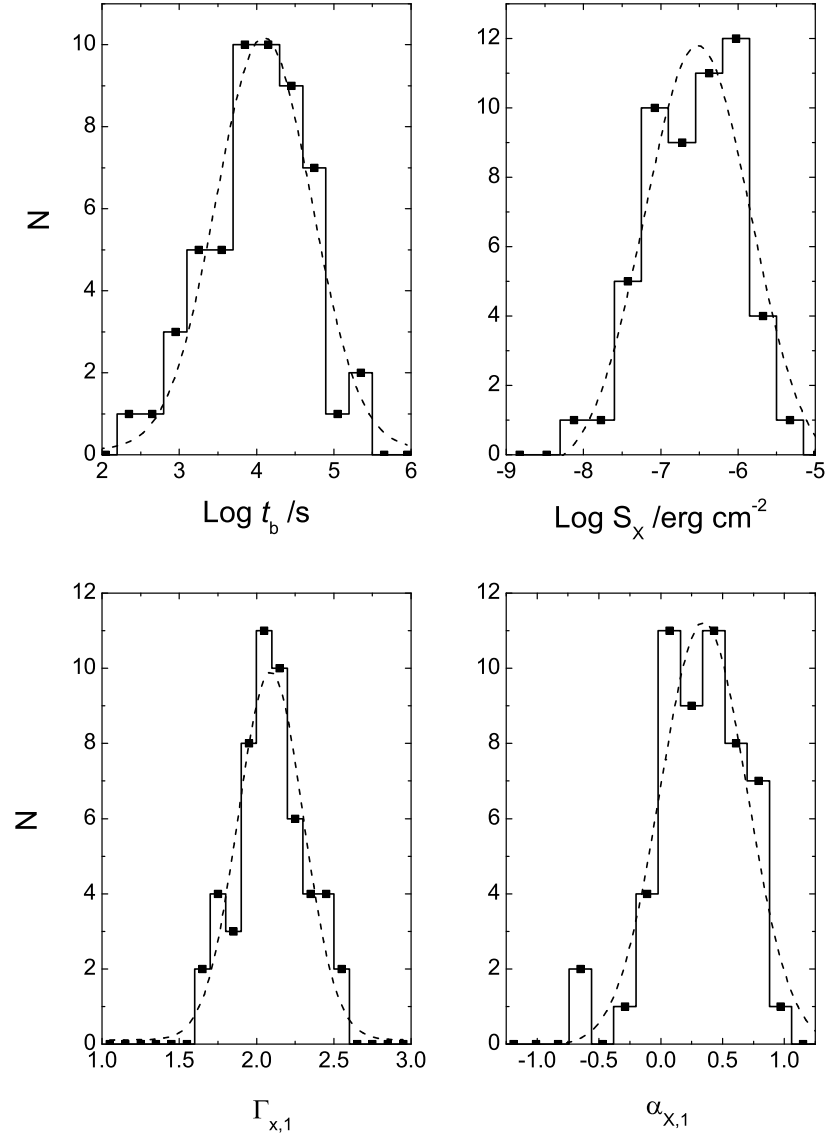


FIG. 3.— Distributions of the characteristics of the shallow decay segment for the bursts in our sample. The dashed lines are the fitting results with Gaussian functions.

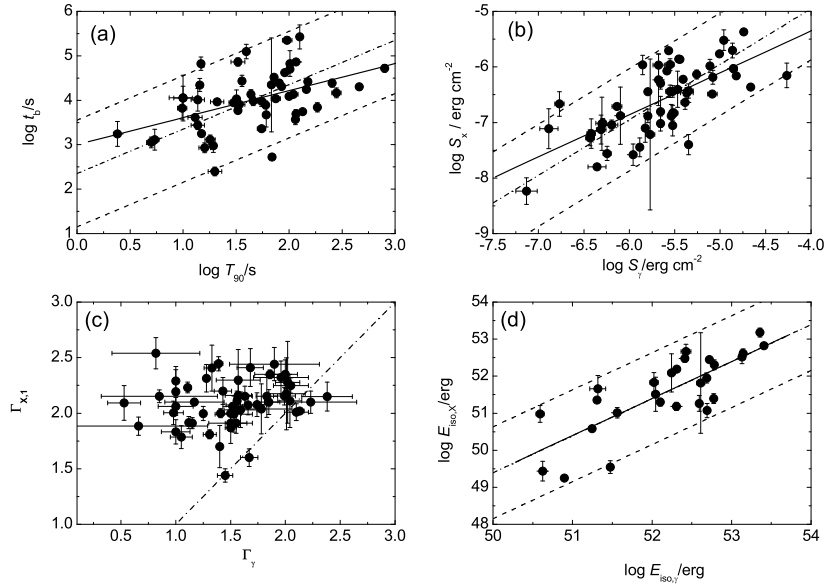


FIG. 4.— The correlations between the data of the shallow decay phase and the prompt gamma-ray phase. The *solid* line in each panel is the best fit. The *dashed* lines mark a 2σ region defined as $y = x + (A \pm 2 \times \sigma_A)$, where y and x are the quantities in the y and x -axes, respectively, and A and σ_A are the mean and its 1σ standard error of $y - x$, respectively. The *dash-dotted* line is $y = x$.

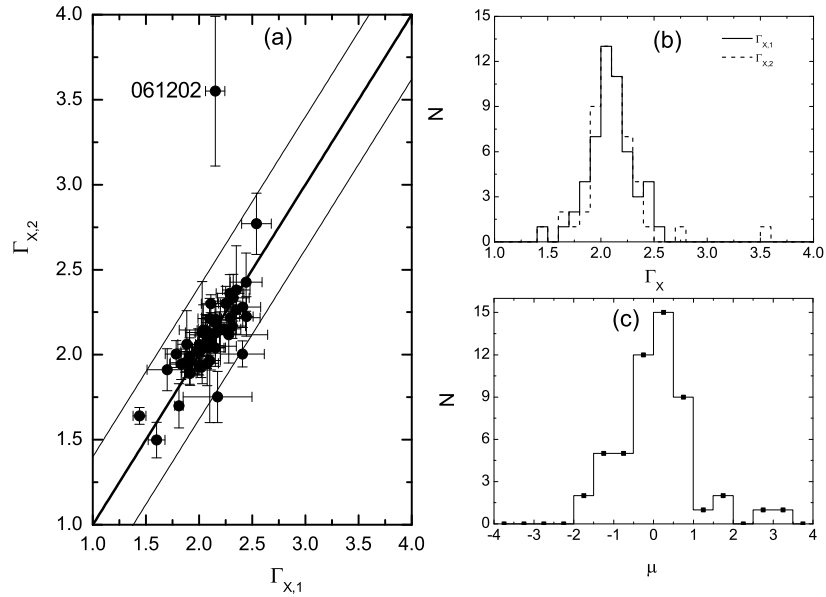


FIG. 5.— The comparison between $\Gamma_{X,1}$ and $\Gamma_{X,2}$: (a) $\Gamma_{X,1}$ vs. $\Gamma_{X,2}$. The *solid* lines marks the equality line $\Gamma_{X,2} = \Gamma_{X,1}$ and its 2σ region; (b) The histograms of $\Gamma_{X,1}$ and $\Gamma_{X,2}$; (c) The distribution of μ .

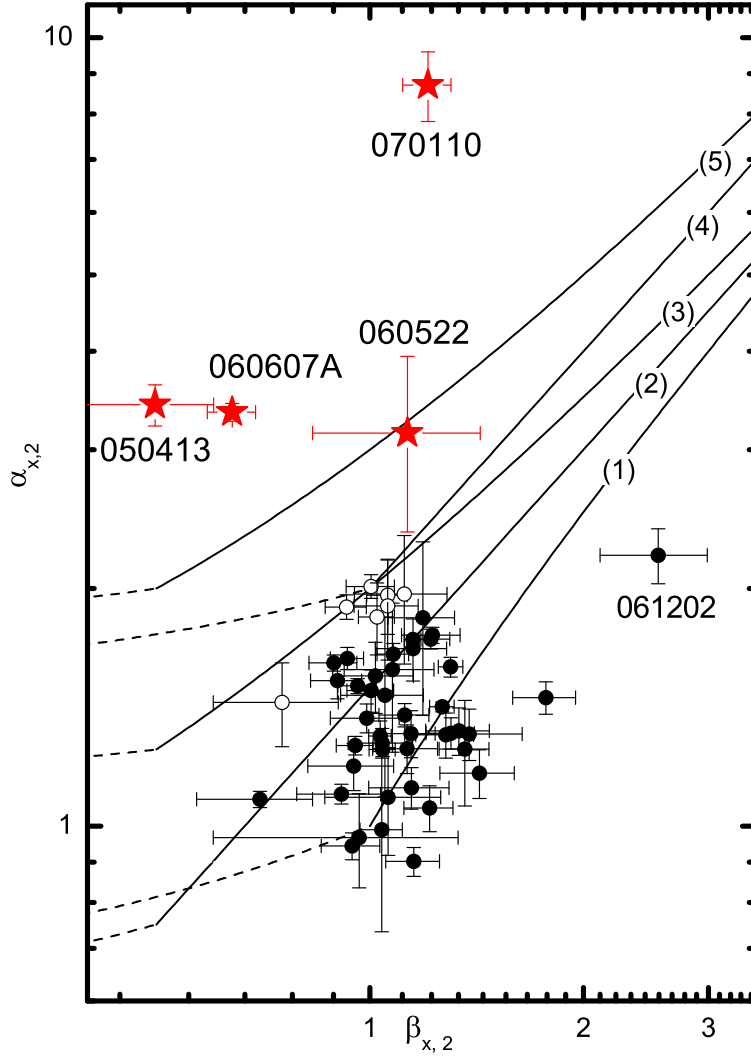


FIG. 6.— The temporal decay index $\alpha_{X,2}$ as a function of the spectral index $\beta_{X,2}$ for the post-break segment as compared with the closure correlations of various external shock afterglow models: (1) $\nu > \max(\nu_c, \nu_m)$; (2) $\nu_m < \nu < \nu_c$ (ISM, slow cooling); (3) $\nu_m < \nu < \nu_c$ (Wind, slow cooling) (4) $\nu > \nu_c$ (Jet, slow cooling) (5) $\nu_m < \nu < \nu_c$ (Jet, slow cooling). The solid lines are those for electron distribution index $p > 2$, and the dashed lines are for $p < 2$. The *solid* dots represent the bursts whose $\alpha_{X,2}$ and $\beta_{X,2}$ satisfy the models (1) and (2), and the open dots represent those bursts can be explained with the model (3). The stars are those bursts that significantly deviate from the external shock afterglow models including 060522 (see discussion in the text).

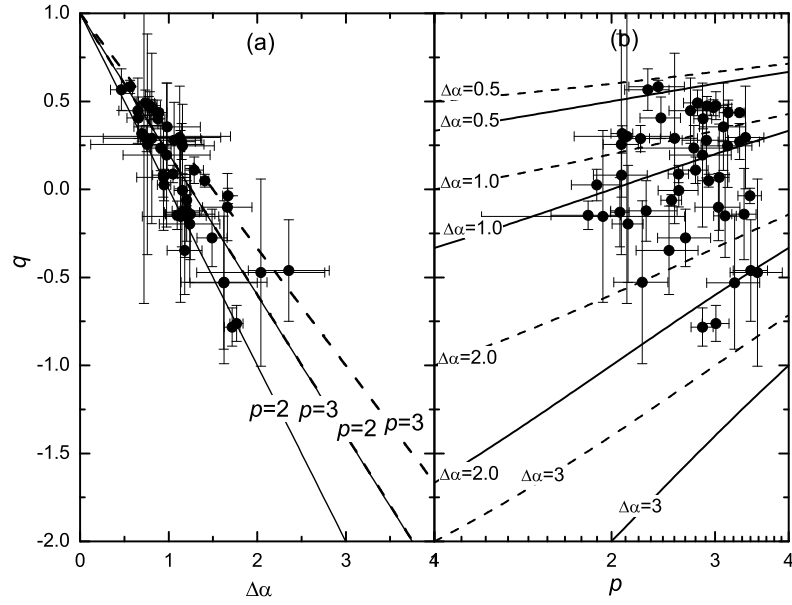


FIG. 7.— The distributions of the 49 GRBs whose normal decay phases are consistent with the external shock models in the $q - \Delta\alpha$ (panel a) and $q - p$ (panel b) planes along with the model predictions for $\nu > \max(\nu_c, \nu_m)$ (solid lines) and $\nu_m < \nu < \nu_c$ (dashed lines).

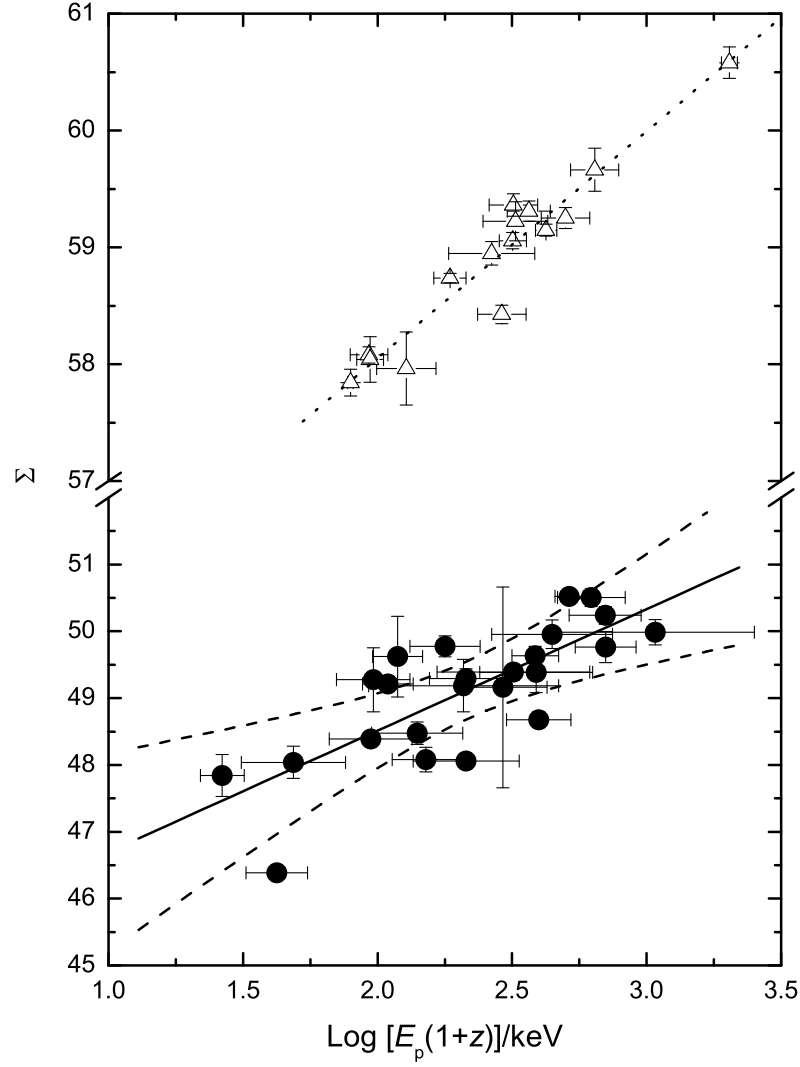


FIG. 8.— Comparison of the $E_{\text{iso},X} - E'_p - t'_b$ relation with the bursts in our sample (the solid dots; the solid and dashed lines mark the best fit in 3σ level) with the Liang-Zhang relation derived with pre-*Swift* bursts (the open triangles and the dotted line is the best fit; Liang & Zhang 2005), where $\Sigma_X \equiv \log E_{\text{iso},X} - \kappa_2 t'_b$ and $\Sigma_\gamma \equiv \log E_{\text{iso},\gamma} - \kappa_2 t'_{b,0}$.